LAJSBA
LATIN AMERICAN JOURNAL OF SEDIMENTOLOGY AND BASIN ANALYSIS | VOLUME 31 (1) 2024, 65-95

DIAGENETIC EVOLUTION OF THE PERMIAN TUNAS FORMATION, CLAROMECÓ BASIN, BUENOS AIRES PROVINCE, ARGENTINA: ITS IMPACT ON POROSITY AND RESERVOIR CHARACTERISTICS

María Belén Febbo[1,2,3], Nora Cesaretti[2], Silvia Omodeo-Salé[1], Andrea Moscariello[1], Antoine de Haller[1], Natalia Fortunatti[2], Giselle Choque[2,3], Renata Tomezzoli[3]*

[1] Department of Earth Sciences, University of Geneva. Rue de Maraichers, 13, CH-1205, Geneva, Switzerland.
[2] Departamento de Geología, Universidad Nacional del Sur (UNS). Avda. Alem 1253, cuerpo B'-1°Piso, B8000CPB, Bahía Blanca, Buenos Aires, Argentina.
[3] Consejo Nacional de Investigaciones Científicas y Técnicas (CONICET), Argentina.
*Corresponding author: belenfebbo@gmail.com

ARTICLE INFO

Article history
Received October 11, 2023
Accepted December 12, 2023
Available online December 29, 2023

Handling Editor
José I. Cuitiño

Keywords
Diagenesis
Reservoir
Tight gas sandstones
QEMSCAN
Claromecó Basin

ABSTRACT

The foreland Claromecó Basin, located in the south-western sector of Buenos Aires province, Argentina, has a relevant economic and energetic interest due to the presence of coal layers contained in the Permian Tunas Formation, which might be considered effective source rock for gas resource generation. This study aims to reconstruct the diagenetic evolution of the Tunas Formation at the Claromecó Basin (PANG 0001 and PANG 0003 wells) and determine how the diagenesis affected the reservoir quality. To this purpose, core samples of the Tunas Formation were analysed using a combination of micro petrographic analyses (transmitted light, QEMSCAN, cathodoluminescence), fluid inclusions studies, and petrophysical methods (conventional core analysis, CCA). The analysed sedimentary successions are composed of sandstones interbedded with mudrocks, carbonaceous mudrocks, tuffs, and coals. Sandstones are medium- to fine-grained, framework-supported, and moderate-to-well-sorted. Authigenic minerals are calcite and laumontite, with minor proportions of quartz and feldspar overgrowths and clay minerals (illite, muscovite, and chlorite). Porosity is of secondary type, generated by fracturing and dissolution of feldspars and carbonate cement. Porosity determined by optical, QEMSCAN, and CCA analyses ranges from 0.1 to 4 %, with a permeability varying between 10^{-3} and 10^{-6} millidarcies. Fluid inclusion studies were performed in sandstone cements and calcite and quartz veins. Primary, pseudo-secondary, and secondary aqueous and organic fluid inclusions were recognized. Organic fluid inclusions show green and light blue fluorescence, which indicates the presence of hydrocarbons. Homogenization temperatures of fluid inclusions obtained from microthermometry studies range from 124 to 200 °C in cements and 110 to 230 °C in veins. These temperatures confirm a metagenesis stage for the Tunas Formation, within the wet to dry gas window. Given the petrophysical characteristics of the analyzed levels, sandstones could be considered unconventional tight gas sandstone reservoirs. Obtained results point out that during early diagenesis, physical compaction and precipitation of carbonate cement are the principal factors that significantly reduce the primary porosity. Furthermore, in the mesogenesis

stage, chemical compaction, calcite and zeolite cements precipitation, and quartz overgrowths further contribute to porosity loss. However, secondary porosity was produced during mesogenesis due to the dissolution of unstable grains and calcite cements caused by the action of acid fluids generated during the decomposition and maturity of organic matter. Additionally, secondary porosity was also generated by fracturing due to burial and tectonic stress and by the increased pore pressure during hydrocarbon generation and migration. The reservoir properties of the Claromecó Basin have been controlled mainly by diagenetic and tectonic processes that acted during the burial history of the basin. Clasts and cements composition also influenced diagenesis together with the presence of organic-rich rocks, which could generate hydrocarbons.

INTRODUCTION

Reservoir quality in sandstones is the product of primary depositional characteristics and secondary diagenetic processes (Worden and Burley, 2003). Primary textural attributes are mainly controlled by grain size, sorting, detrital clay content and distribution of clasts (Beard and Weyl, 1973; Blatt *et al.*, 1980; Cade *et al.*, 1994). Diagenetic processes are governed by the provenance of clastic material, depositional mineralogy, diagenesis of organic matter and clay fraction, chemical changes in pore fluids, temperature and pressure during burial, and tectonic stress (Blatt, 1979). During early diagenesis, processes like mechanical compaction, precipitation of early calcite cements and siliceous syntaxial growths occur, contributing to primary porosity loss (Choquette and Pray, 1970; Surdam *et al.*, 1989). During mesogenesis, chemical compaction further reduces porosity, leading to pressure dissolution of silicates and subsequent precipitation of silica cements (Blatt, 1979; Surdam *et al.*, 1989). On the other hand, diagenesis can increase the porosity of the rock by secondary porosity generation through dissolution or fracturing. A detailed analysis of the processes involved in the diagenetic history of a sedimentary sequence is therefore essential to characterize the porosity and permeability of the rock and thus, to identify potential reservoirs for hydrocarbons, CO_2 or H_2 storage, or geothermal fluids.

The foreland, late Paleozoic Claromecó Basin, located in southern Buenos Aires province (Fig. 1a), Argentina, has attracted exploration interest from the oil industry over the last decades due to the presence of subsurface coal beds which might represent a target for conventional and/or unconventional gas resources (Lesta and Sylwan, 2005; Arzadún *et al.*, 2017; López-Gamundi and Rossello, 2021; Febbo *et al.*, 2022a; Febbo, 2023). These coal-bearing levels can be correlated with Permian Gondwana coals of the Rio Bonito Formation (Paraná Basin, Brazil; Kalkreuth *et al.*, 2006; Holz *et al.*, 2010; Mendonça Filho *et al.*, 2013) and the Karoo Supergroup (Karoo foreland Basin; South Africa; Geel *et al.*, 2015), which have become important exploration targets. Additionally, in recent years the coal seams and sandstones levels of the Claromecó Basin are considered as potential targets for CO_2 storage (Grasetti *et al.*, 2022; Molina *et al.*, 2023).

Hydrocarbon exploration in Buenos Aires province began in the 1990s through gravimetric studies, seismic data, and onshore exploration wells. Several coal beds up to 11 m-thick were drilled, belonging to the Early Permian Tunas Formation (Harrington, 1947; Lesta and Sylwan, 2005). Coal deposits of the PANG 0001 (S37° 40.8' 17.0", W61° 11.30' 06") and PANG 0003 wells (S37° 34.0' 44.24", W61° 22.0' 12.56") (Fig. 1b) were previously studied to evaluate the hydrocarbon potential of this unit. Total organic carbon (TOC%) content in carbonaceous lithologies is high, between 0.5 and 2 % in organic-rich shales, and from 26 to 53.9 % in carbonaceous shales and coals (Febbo *et al.*, 2022a; Febbo, 2023). Based on these values, coal-bearing layers are characterized as good-quality source rocks (Febbo *et al.*, 2022a). The organic matter identified in the coals is of terrigenous origin and belongs to type III and type IV kerogens (Arzadún *et al.*, 2017; Febbo *et al.*, 2022a, 2023; Febbo, 2023). Vitrinite reflectance (%Ro) values range from 1.45 to 2.8 % (Arzadún *et al.*, 2017; Febbo *et al.*, 2023), reflecting a catagenesis

to late catagenesis stage within the wet to dry gas window. Therefore, organic matter quantity, type, and maturity, suggest that the carbonaceous levels of the Tunas Formation have a good potential as gas-prone source rocks (Arzadún *et al.*, 2017; Febbo *et al.*, 2022a). Moreover, preliminary subsurface and outcrops studies point out the potential of the naturally fractured sandstone beds of this unit as hydrocarbon reservoirs (López-Gamundi and Rossello, 2021; Choque *et al.*, 2021; Febbo, 2023). Based on this scenario, an exhaustive study of the diagenetic processes and petrophysical parameters of the Tunas Formation sandstones is necessary to identify and characterize potential reservoir levels.

This study aims at reconstructing the diagenetic evolution of the Tunas Formation in the Claromecó Basin (PANG 0001 and PANG 0003 wells) and determining how the diagenesis affected its reservoir quality. To this purpose, core samples of the Tunas Formation (Fig. 1) were analysed by combining mineralogy and petrography studies (transmitted light, QEMSCAN, cathodoluminescence, X-ray diffraction), fluid inclusions analyses, and petrophysical methods (conventional core analysis, CCA). Sandstone samples were studied in detail to characterize the reservoir. Mudrocks and tuffs interstratified with sandstones were investigated to assess whether the composition of the fine-grained rocks influence on the diagenetic processes that affected the reservoir (i.e., cement composition). The results obtained provide a better understanding of the relationship between diagenesis and preservation of reservoir parameters during the basin history and decrease uncertainties for the exploration of potential conventional and/or unconventional gas resources in Argentina.

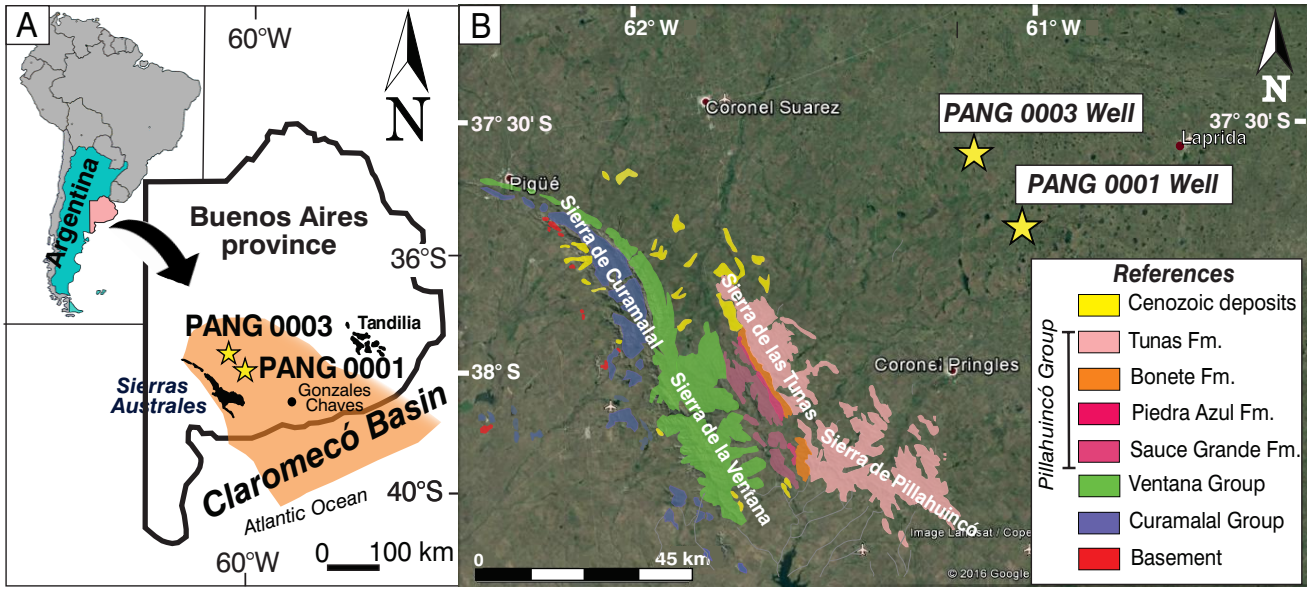

Figure 1. a) Location of the Claromecó Basin, Sierras Australes System, and PANG 0001 and PANG 0003 wells, located at the basin center; **b)** Location of the PANG 0001 and PANG 0003 wells and geological map of the Sierras Australes System, modified from Suero (1972).

GEOLOGICAL SETTING

The foreland Claromecó Basin (Carboniferous–Permian; Ramos, 1984) extends for about 65000 km^2 from the Sierras Australes System (southern Buenos Aires province) to the argentinean continental shelf (Fig. 1a). The basin was defined by gravimetric studies, with a maximum sedimentary thickness of 9 to 10.5 km (Introcaso, 1982; Kostadinoff and Prozzi, 1998; Kostadinoff, 2007). This basin was formed during the Gondwanides orogeny (Permian–Triassic; Keidel, 1916 Du Toit, 1927; Milani and De Wit, 2008), linked with the collision of the Patagonia terrain with southwestern Gondwana margin during the Late Paleozoic (Ramos, 2008; Tomezzoli, 2012; Pángaro and Ramos, 2012; Ramos and Naipauer, 2014).

The study area can be divided into two sectors: the southwest portion, which comprises the highly deformed sequences of the Ventana, Curamalal, and

Pillahuincó Groups (Harrington, 1947), exposed in the Sierras Australes System (Fig. 1b), and the northeast zone, which encompasses the foreland area, with weak deformation and horizontal strata (von Gosen *et al.*, 1991; Ramos and Kostadinoff, 2005). Therefore, a decrease in deformation is recorded in the Paleozoic sequences towards the east, where the Curamalal and Ventana groups display a lower greenschist metamorphism, while the Pillahuincó Group present a very low-grade metamorphism to high diagenesis (Fig. 1b; Buggisch, 1987; von Gosen *et al.*, 1991). Anisotropy of magnetic susceptibility (AMS) performed on Tunas Formation outcrops (Tomezzoli, 2001; Arzadún *et al.*, 2016, 2021) and subsurface records (Febbo *et al.*, 2021) confirm a decrease in the magnitude of tectonic deformation towards the east-northeast during the Early late Permian.

The Claromecó Basin fill is represented by the Carboniferous to Early Permian Pillahuincó Group (Harrington, 1947), cropping out in the eastern portion of the Sierra Australes System, and continues to the east in subsurface, where it is covered by Cenozoic deposits (Fig. 1b). The group is subdivided into four formations that from base to top are the Sauce Grande, Piedra Azul, Bonete, and Tunas (Fig. 1b), with a maximum thickness of 2800 m (Harrington, 1947). The Tunas Formation is the youngest unit and represents the last stage of the Paleozoic basin infill. This unit is exposed from the north of Sierra de las Tunas to the south of Sierra de Pillahuincó (Fig. 1b), and continues in subsurface to the east, whit the exception of small and isolated Permian outcrops located near Gonzales Chavez locality (Fig. 1a-b; Monteverde, 1937; Furque, 1965; Harrington, 1970; Febbo *et al.*, 2022b). The exposed thickness ranges from 600 to 2400 m with many uncertainties given its lithological homogeneity and tectonic complexity (Harrington, 1970; Suero, 1972; Andreis and Japas, 1991; Vazquez Lucero *et al.*, 2020). The Tunas Formation deposits consist of fine- to medium- grained greenish and yellowish sandstones with cross-stratification, interbedded with laminated greenish mudrocks and thin pyroclastic beds (Harrington, 1947, 1970; Andreis *et al.*, 1979; López-Gamundi, 1996, 2006; Zavala *et al.*, 1993; Alessandretti *et al.*, 2013; Arzadún *et al.*, 2018; Febbo *et al.*, 2022b). Towards the foreland basin area, this unit is well documented in the PANG 0001 (S37° 40.8' 17.0", W61° 11.30' 06") and PANG 0003 (S37° 34.0' 44.24", W61° 22.0' 12.56") exploration wells (Figs. 1a-b), with a maximum thickness of 700 m. There, the unit consists of medium to fine-grained sandstones, interbedded with black organic rich mudrocks, heterolites, greenish mudrocks, tuff layers, carbonaceous mudrocks, and coals (Arzadún *et al.*, 2017; Zavala *et al.*, 2019; Febbo *et al.*, 2021, 2022a, b; Febbo, 2023; Choque *et al.*, 2021, 2022). The age of this unit is Early Permian (Sakmarian–Artinskian) based on *Glossopteris* flora (Archangelsky and Cúneo, 1984; Cúneo, 1996) and U–Pb ages obtained from outcropping (280–291 Ma; Tohver *et al.*, 2008; López-Gamundi *et al.*, 2013; Alessandretti *et al.*, 2013; Arzadún *et al.*, 2018) and subsurface (PANG 0001 well, 295.5 ± 8.0 Ma; Arzadún *et al.*, 2018) pyroclastic layers. These ages are consistent with palynological data from core samples of the PANG 0001 well (di Pasquo *et al.*, 2018).

The Tunas Formation sediments were deposited in deltaic to fluvial environments (Andreis *et al.*, 1989; Andreis and Japas, 1991; Zavala *et al.*, 1993; Ballivián Justiniano *et al.*, 2020), representing the culmination of a regressive cycle after shallow marine conditions registered in the Piedra Azul and Bonete formations (Harrington, 1947). Subsurface facies of the Tunas Formation (PANG 0001 and PANG 0003 wells) are interpreted as a river-dominated deltaic environment (Zavala *et al.*, 2019). These authors defined transgressive-regressive cycles represented by lower delta-plain deposits, composed of coals and shales, which progressively change towards the upper section to sandy and heterolithic delta front and shelf deposits.

Based on the occurrence of growth strata (López-Gamundí *et al.*, 1995, 2013) and paleomagnetic data (Tomezzoli, 1999, 2001) the Tunas Formation was interpreted as a synorogenic unit. This unit records sedimentation in a foreland basin developed along an active margin, characterized by paleocurrents reversal and the dominance of fold belt/arc-derived material (López-Gamundí *et al.*, 1995, 2013; Alessansretti *et al.*, 2013; Febbo *et al.*, 2022b). The sedimentation was contemporary with explosive volcanic activity evidenced by tuffs interbedded with clastic material which confirms an Early Permian volcanism in the southwestern Gondwana margin (Alessandretti *et al.*, 2013; López-Gamundí *et al.*, 2013; Arzadún *et al.*, 2018; Ballivián Justiniano *et al.*, 2020; Febbo *et al.*, 2022b).

METHODOLOGY

Sandstone petrography

Petrographic and diagenetic analyses were performed on 33 thin sections (24 sandstones, 8 mudrocks, and 1 tuff) of the Tunas Formation belonging to different stratigraphic levels of the PANG 0001 and PANG 0003 wells (Figs. 2-3). Standard optical microscopy analyses were performed with a Nikon Eclipse 50i POL microscope. The modal composition of sandstones was determined according to the Gazzi-Dickinson method, counting 350 grains per sample. Grains were counted using the JMicroVision software point counter. Sandstones were classified according to Folk *et al.* (1970) based on their quartz, feldspar, and lithic content, recalculated to 100% (Table 1). Detrital constituents in the framework, percentage of matrix, porosity, and cement were quantified by visual microscopic analysis and QEMSCAN® (Table 1). Compton's (1962) comparators descriptors were used to define sorting characteristics.

Automated mineral and textural characterization were performed with FEI QEMSCAN on 21 polished and carbon-coated thin sections (Figs. 2-3) at the Department of Earth Sciences, University of Geneva (Switzerland). QEMSCAN technology acquires energy-dispersive X-ray spectra and backscattered-electron image information from each measurement point and identifies the underlying minerals using the chemical composition from X-ray information preferentially over backscatter-electron brightness (Gottlieb *et al.*, 2000). Analyses were carried out under high vacuum conditions (10−6 mbar) an acceleration voltage of 15 kV with a probe current of 10 nA. The acquisition time of the energy-dispersive X-ray signal was approximately 200 pixels per second using a point spacing of 5 μm. Mineral-phase identification was automatically performed by comparing energy-dispersive X-ray spectra of individual pixels with a database of standard spectra using the FEI iDiscover™ software. In order to obtain an acceptable final result, energy-dispersive X-ray spectra and elemental concentrations were compared with available databases. The database was then refined by microscopic observations. For each sample, a scan image was produced showing all identified minerals. The abundance of each mineral was finally estimated by quantifying its occurrence as surface percentages.

Representative samples from fine-grained lithologies and sandstones were collected to perform X-Ray diffraction (XRD) analyses in order to determine their mineralogy (Figs. 2, 3). XRD analyses were done using a Rigaku D-Max III-C diffractometer, Kα of Cu radiation, with a voltage of 30 kV, current of 15 mA, and scan of 2º per minute. The analyses were performed at the facilities of the Departamento de Geología, Universidad Nacional del Sur (Argentina).

Diagenetic features

Diagenetic features and cross-cutting relationships were examined using conventional thin-section petrography, cathodoluminescence microscopy, and QEMSCAN. The type of grain-to-grain contact (floating, tangential, long, concavo-convex, or sutured) and the intensity of compaction were described for each sample, based on Talylor (1950).

Cathodoluminescence analysis was conducted on 11 selected polished thin sections (Figs. 2-3) at the facilities of the Departamento de Geología, Universidad Nacional del Sur (Argentina), in order to better characterize the diagenetic features (cement and dissolution). The studies were performed under a Nikon Eclipse 50i POL microscope coupled to a MK5- 2 (CITL CL5) cathodyne. The beam conditions were 10 to 15 kV at 250 mA of current.

For porosity determinations, 14 thin sections were impregnated with blue epoxy to distinguish the pores from the frameworks (Figs. 2-3). Porosity classification is based on Schmidt and Macdonald (1979). Porosity was quantified using the JMicroVision software from petrographic images (visual porosity) and QEMSCAN, considering the percentage of background (resin) in each sample (Figs. 2-3). In addition, standard petrophysical porosity and gas permeability studies (conventional core analysis, CCA) were performed on 4 samples from the PANG 0003 well (Fig. 3) at the LCV Laboratory (Florencio Varela, Argentina). The latter provided a three-dimensional quantitative porosity percentage that could be compared with values obtained by two-dimensional optical microscopy and QEMSCAN.

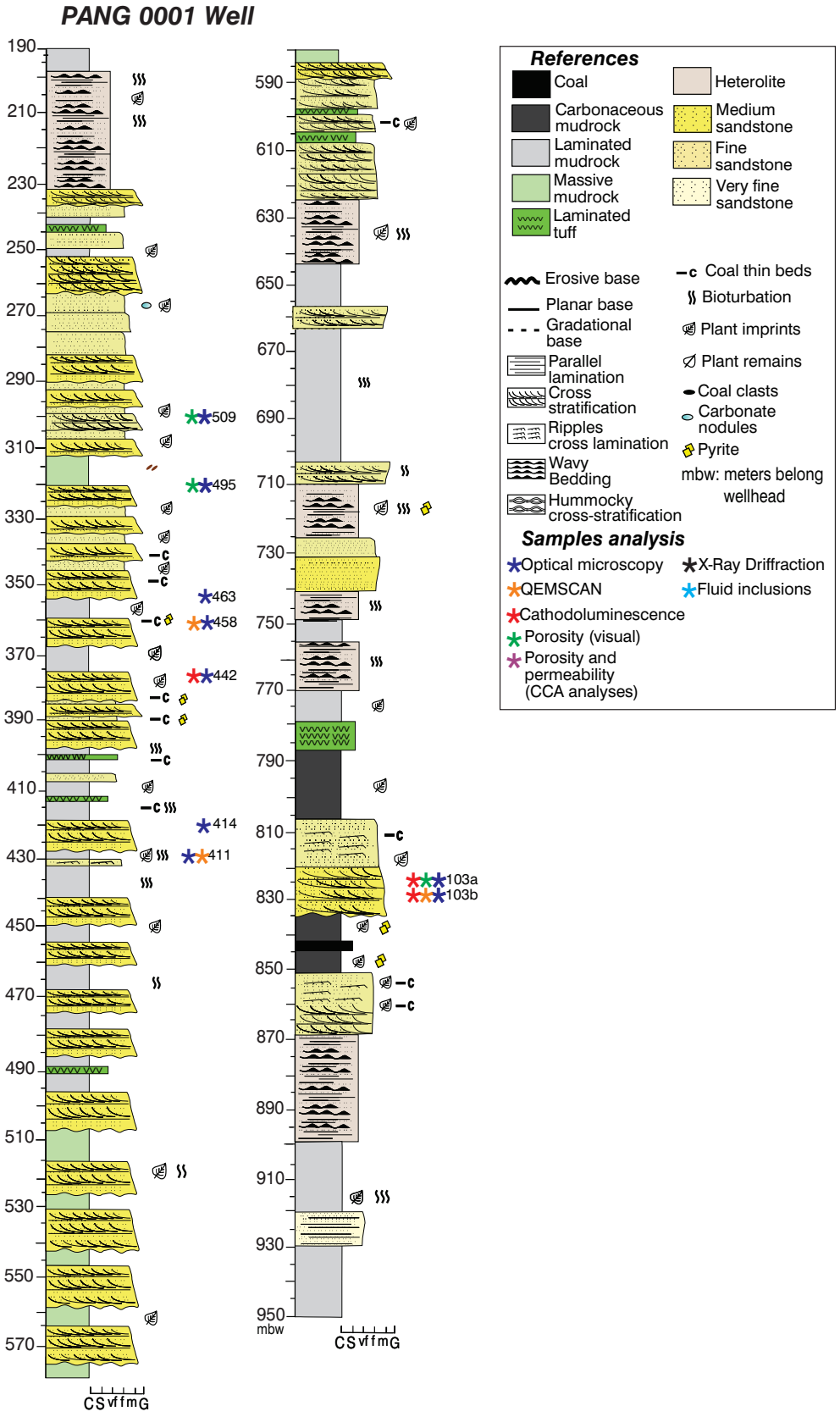

Figure 2. Sedimentary profile of the Tunas Formation in the PANG 0001 well, Claromecó Basin, modified from Arzadún *et al.* (2017), showing the stratigraphic position of the studied samples. Analyses performed in each sample are represented by different colors (see references).

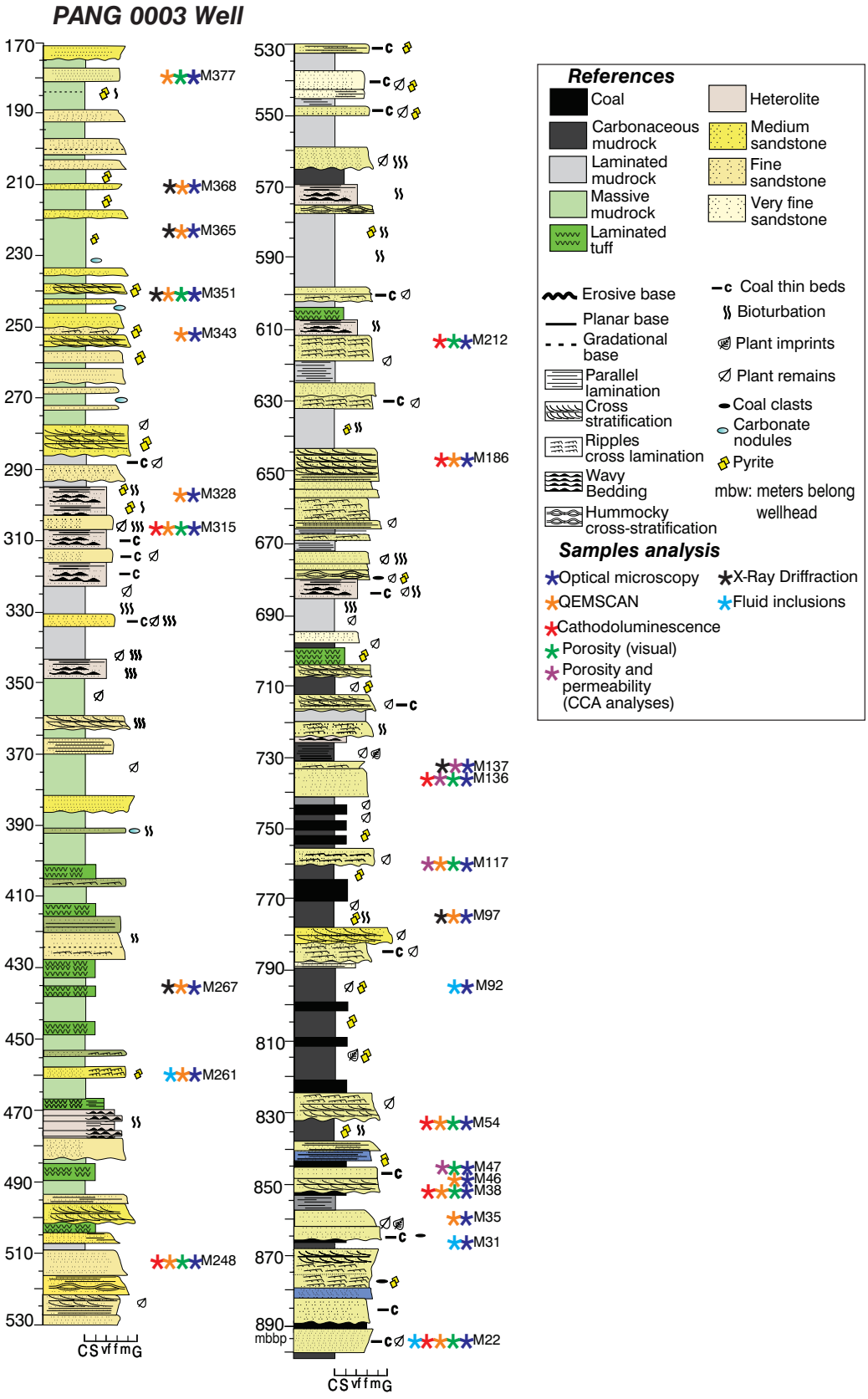

Figure 3. Sedimentary profile of the Tunas Formation in PANG 0003 well, Claromecó Basin and stratigraphic positions of studied samples. Analyses performed in each sample are represented by different colors (see references).

Fluid inclusions analysis

Fluid inclusion (FI) petrography and microthermometry analyses were performed in sandstones and mudrock samples (Figs. 2-3). The studies were conducted at the Luminescence Laboratory of the Departamento de Geología, Universidad Nacional del Sur (Argentina), with a Nikon eclipse 50i POL polarization microscope. Fluorescence studies were executed under ultraviolet incident light (UV), with a Nikon 100W mercury lamp (halogen) to identify aqueous and organic (hydrocarbon-bearing) inclusions. Criteria of Riecker (1962) and Burruss (1981) were used to determine the presence and type of hydrocarbons trapped within the inclusions from their fluorescence color. Fluid inclusions were classified according to their origin as (1) primary, (2) pseudo-secondary, and (3) secondary, based on Roedder (1984). Microthermometry analyses were carried out on 4 doubly polished thin sections (Fig. 3). The fluid inclusions studied were situated in diagenetic cements (calcite and quartz overgrowths) and quartz and calcite veins. Measurements were conducted with a Linkam MDS 600 programmed heating/freezing stage, which can examine the phase temperatures between the -180° and 600 °C, coupled on an Olympus BX50 petrographic microscope, available at the Departamento de Geología, Universidad Nacional del Sur (Argentina). Heating analyses were performed in primary and pseudo-secondary two-phase (liquid-vapor) inclusions, according to procedures establish by Goldstein and Reynolds (1994), from room temperature (23 °C) to 200 °C and even 240 °C.

RESULTS

Petrographic features

Petrographic and diagenetic analyses were conducted on core samples of the PANG 0001 and PANG 0003 wells (Figs. 2-3). The analysed succession for each well present a thickness of ~700 m and present similar facies successions. The lower levels of both sections consist of thin, medium- to fine-grained sandstones, followed by thick packages of carbonaceous mudrocks and coal beds of up to 25 m-thick with abundant pyrite nodules and plant remains (Figs. 2-3). Toward the top of the columns, coal strata become thinner and gradually disappear, replaced by thick packages (~20 m) of medium- to fine-grained sandstones, with irregular bases, cross-bedding stratification, and abundant plant remains interbedded with greyish laminated mudrocks and thin tuff layers (Figs. 2-3). The upper levels are characterized by greenish laminated mudrocks and medium to fine-grained sandstones, interbedded with intensely bioturbated mudrocks, heterolites, fine-grained sandstones, and thin coal beds (1-5 cm) (Figs. 2-3).

Mineralogical and textural composition of sandstones were determined by optical microscopy and QEMSCAN (Figs. 4a, 5, 6). Sandstones classify as feldspathic litharenite (78 %), lithic feldsarenite (17 %) and litharenite (5 %) (Fig. 5, Table 1). The detrital fraction is dominated by quartz (comprising 38 to 57 % of the total main components), feldspar (comprising 11 to 35 %) and lithic fragments (comprising 25 to 47 %) (Fig. 5, Table 1). Grain size varies from medium (1 mm) to very fine (0.062 mm), mostly with a medium to fine size. Sandstones are framework-supported, composed of moderate to well sorted, sub-rounded to sub-angular grains with long to concavo-convex contacts. The matrix content is between 10 and 20 %, composed of quartz, lithic rock fragments and clay minerals (illite and micas).

Quartz occurs as monocrystalline or polycrystalline grains, with an average of 47 % (Figs. 6a-b, Table 1). The quartz content fairly remains constant, slightly increasing towards the base of the successions (Fig. 4a). Grains have sub-rounded to sub-angular shapes with straight and occasionally undulatory extinction.

Feldspars include potassium feldspar and plagioclase, with an average of 20 % (Figs. 6c-d, Table 1). The feldspar content remains fairly constant, increasing slightly towards the top of the successions (Fig. 4a). Plagioclase usually exhibit polysynthetic twinning and sub-tabular shapes (Fig. 6c). Potassium feldspar is represented by orthoclase and microcline (Figs. 6c-d). The orthoclase is usually untwined, with sub-tabular shapes (Fig. 6c) while microcline exhibits tartan twinning, with sub-tabular shapes (Fig. 6d). Feldspars are commonly replaced by clay minerals (Fig. 6e) or albite (Fig. 6d).

Lithic fragments include metamorphic, sedimentary, and volcanic rock fragments, with an average of 33% (Figs. 6a, f-h, Table 1). Metamorphic and sedimentary rock fragments are dominant at

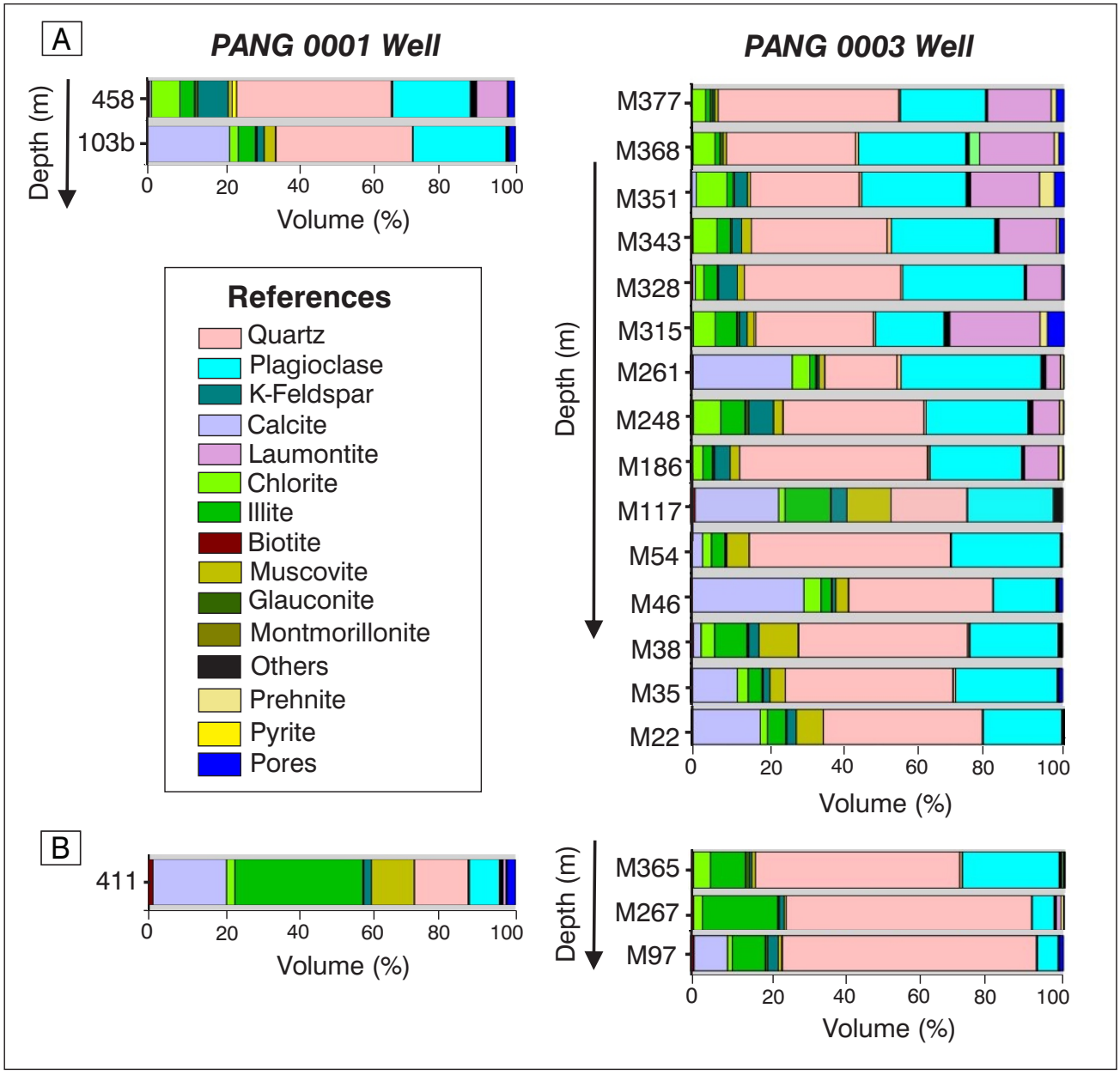

Figure 4. Mineralogical composition of **a)** sandstones and **b)** mudrcoks and tuffs of the Tunas Formation obtained by QEMSCAN (see Figs. 2 and 3 for sample location). The mineralogy of sandstones remains constant throughout both sections, whereas cement composition vary from calcite in the lower to middle part to laumontite in the upper part.

the basal and middle portion of the successions, while volcanic clasts increase in content toward the upper part. Metamorphic lithic fragments have low to medium grade, comprising shales, slates, schists, and quartzites (Figs. 6a, f). Grains show sub-angular shapes. Sedimentary rock fragments include claystones, siltstones, and very fine-grained sandstones, with sub-angular to sub-rounded shapes (Fig. 6g). Volcanic fragments present microlithic and vitrophyric textures (Fig. 6h) and sub-rounded shapes. Lithic fragments are commonly altered and replaced by clays (Fig. 6e).

Accessory minerals comprise from 1 to 5 % of the total main components. They mainly consist of micas, illite, pyrite, epidote, glauconite, and prehnite (Fig. 4a). Sandstones occasionally contain dispersed organic matter.

Mineralogical and textural composition of fine-grained lithologies (mudrocks and tuffs) were determined by optical microscopy, QEMSCAN, and

XRD (Fig. 4b, 7, 8). According to their grain size, mudrocks classify as claystones and argillaceous siltstones. Mineral composition consists of quartz, feldspar, muscovite, biotite, chlorite, and illite (Figs. 4b, 7a-c, 8a). The presence of pyrite and dispersed organic matter is common (Fig. 7b). Tuffs are composed of quartz, feldspar, and clay minerals, mostly illite (Figs. 4b, 6d-f, 8b). The presence of sedimentary lithic fragments is common (Fig. 7e). The matrix is sometimes altered and replaced by calcite (Fig. 8b). Mudrocks and tuffs often have open fractures and calcite and quartz veins (7b-c, f).

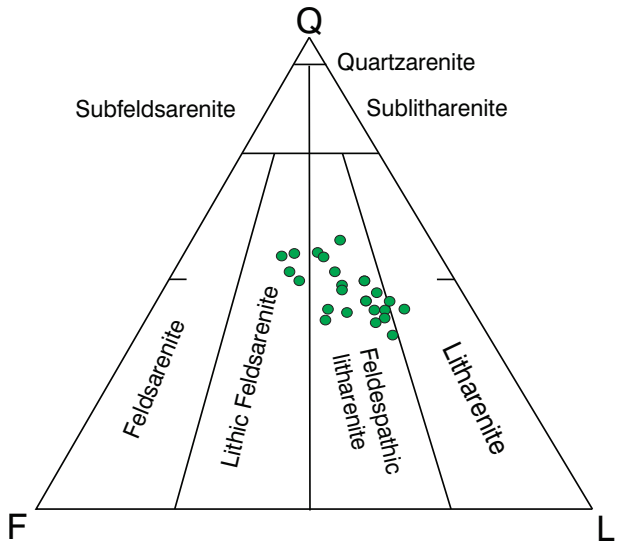

Figure 5. Classification of the Tunas Formation sandstones according to Folk et al. (1970) diagram. Q: Quartz, F: Feldspar, L: Lithic fragments.

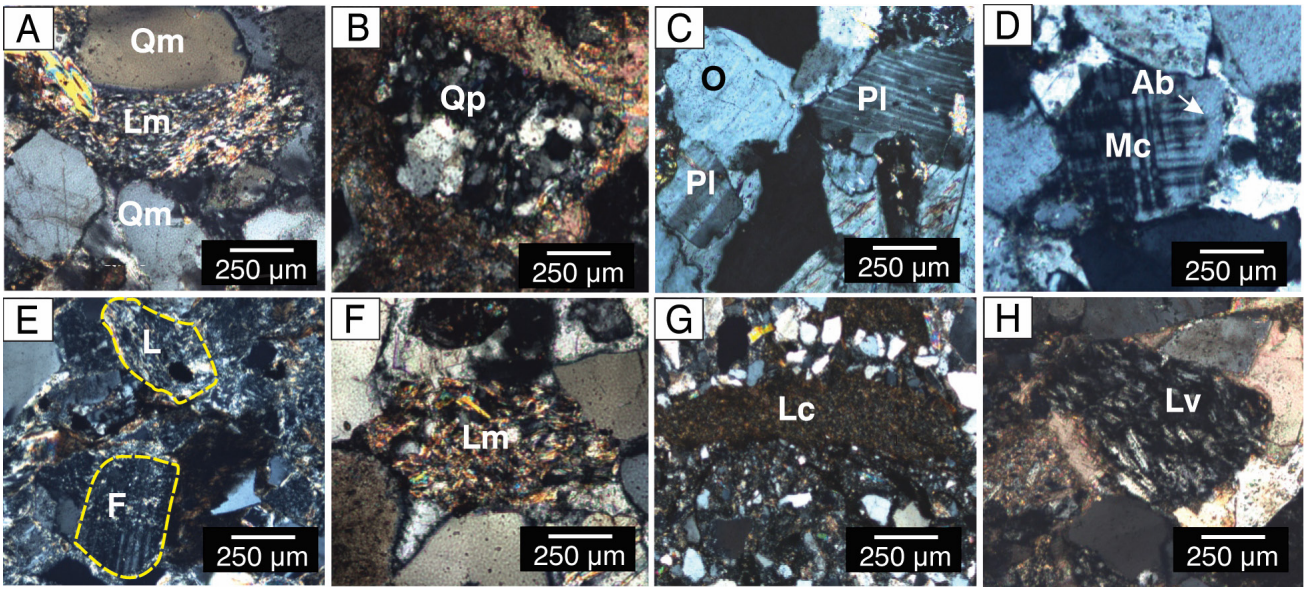

Figure 6. Thin-section photomicrographs of framework components of Tunas Formation sandstones under transmitted light. **a)** Monocrystalline quartz (Qm) and metamorphic lithic fragment (Lm); **b)** Polycrystalline quartz (Qp); **c)** Orthoclase (O) and plagioclase (Pl); **d)** Microcline (Mc) with tartan twining, partially replaced by albite (Ab); **e)** Lithic fragment (L) and feldspar (F) altered by clays; **f)** Metamorphic lithic fragment (Lm); **g)** Claystone lithic fragment (Lc); **h)** Volcanic lithic fragment (Lv).

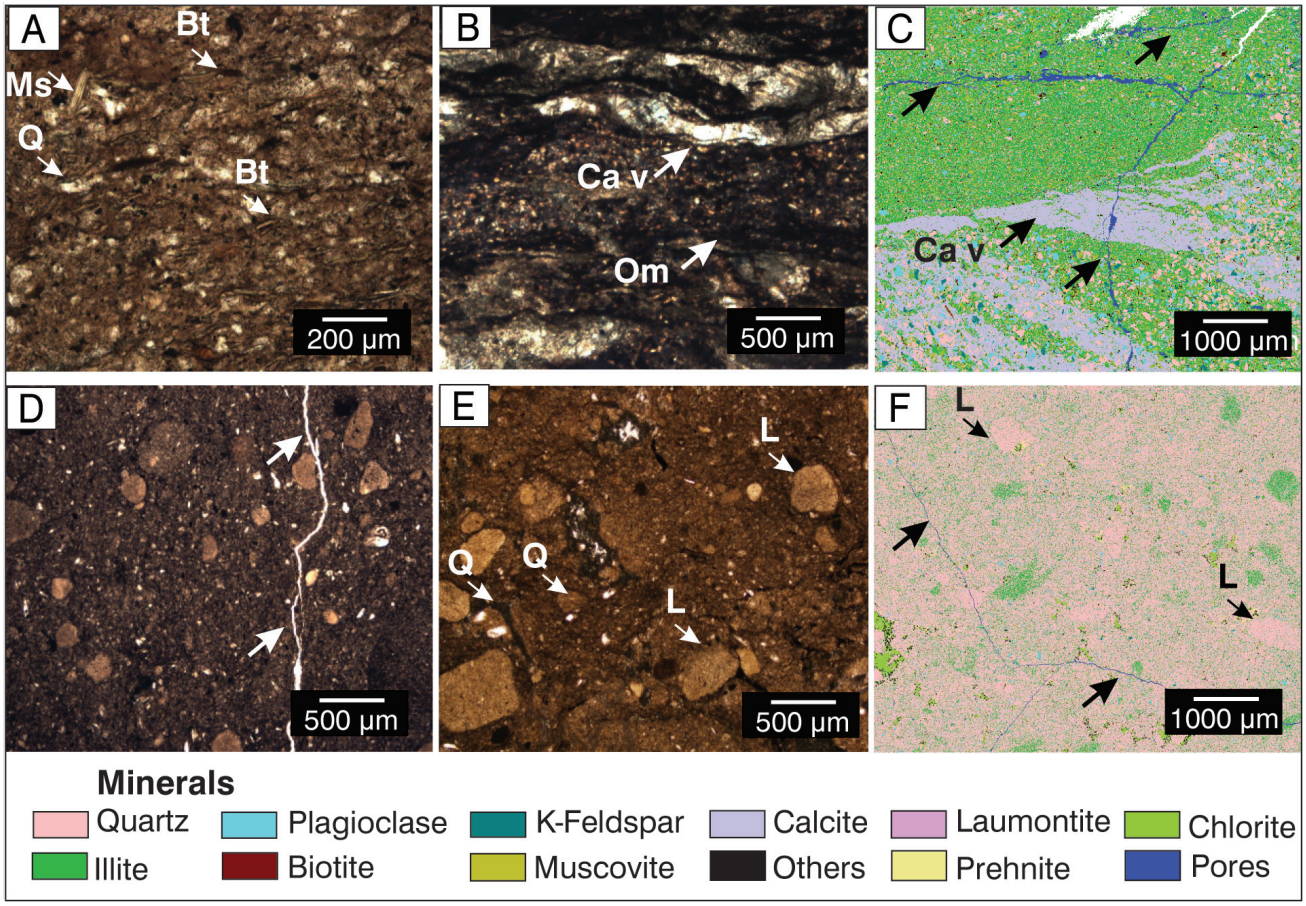

Figure 7. Thin-section photomicrographs of fine-grained lithology under transmitted light (a-b, d-e) and QEMSCAN (c, f). **a-c)** Mudrocks showing quartz (Q), biotite (Bt), muscovite (Ms), calcite veins (Ca vn), and dispersed organic matter (Om); **d-f)** Tuffs showing quartz (Q) and lithic fragments (L). c, d, f) Open fractures are common (indicated by arrows).

Well	Sample	Depth	QFL (%)			Folk *et al.* (1970)'s classification	Main components			
			Q	**F**	**L**		**Clasts (%)**	**Matrix (%)**	**Cement (%)**	**Pores (%)**
PANG 0001	509	304.6	48.7	20.3	31.0	Feldspathic litharenite	85	5	10	<1
	495	323.2	44.6	14.5	40.9	Feldspathic litharenite	80	5	15	<1
	458	365.6	47.7	20	32.3	Feldspathic litharenite	83	10	7	-
	442	382.5	38.0	15.0	47.0	Feldspathic litharenite	85	10	5	-
	414	419.3	43.5	11.0	45.5	Litharenite	85	10	5	-
	103a	822.8	46.9	14.4	39.7	Feldspathic litharenite	85	10	5	<1
	103b	821.5	44.5	18.0	37.5	Feldspathic litharenite	73	7	20	-

PANG 0003	M377	182.4	55.0	25.0	20.0	Feldspathic litharenite	81	5	14	<1
	M368	198.9	54.5	27.5	18.0	Lithic Feldsarenite	74	6	20	-
	M351	239.6	51.3	28.5	20.2	Lithic Feldsarenite	78.5	5	15	1.5
	M343	251.5	48.2	27.6	24.2	Lithic Feldsarenite	76	11	13	-
	M315	311.5	40.9	26.5	32.6	Lithic Feldsarenite	86	5	9	-
	M261	492.6	42.5	25.5	32.0	Feldspathic litharenite	68	7	25	-
	M248	516.3	51.0	20.0	29.0	Feldspathic litharenite	86	7	7	-
	M212	601.0	53.5	20.5	26.0	Feldspathic litharenite	82.6	9	6	2.4
	M186	648.9	57.8	15.3	26.9	Feldspathic litharenite	83	7	10	-
	M137	732.5	41.0	15.9	43.1	Feldspathic litharenite	75	7	18	-
	M136	732.0	43.0	13.9	43.1	Feldspathic litharenite	68	3	25	4
	M117	757.2	50.0	15.0	35.0	Feldspathic litharenite	70	8	22	-
	M54	838.3	43.6	16.4	40.0	Feldspathic litharenite	90	5	5	-
	M47	846.3	44.6	13.0	42.4	Feldspathic litharenite	87.5	7	5	0.5
	M38	854.8	54.2	20.8	25.0	Feldspathic litharenite	81	15	4	-
	M22	879.9	43.0	22.5	34.5	Feldspathic litharenite	77	5	18	-

Table 1. Major detrital components, classification, and percentages of the main components (clasts, matrix, cement, and pores) of the Tunas Formation sandstones, recalculated to 100%. Q: Quartz, F: Feldspar, L: Lithic fragments. Only visual porosity values were included (see Table 2 for details of porosity values).

Diagenetic features

Diagenetic processes involved during the diagenetic history of the Tunas Formation sandstones are mechanical and chemical compaction, precipitation of authigenic minerals as cement, partial or complete replacement of clasts, alteration and dissolution of unstable grains, and fracturing.

Compaction. The sandstones studied display considerable compaction effects. Brittle clasts such as quartz and feldspar are found fractured (Fig. 9a) whereas ductile grains as micas appear bent around resistant detrital grains (Figs. 9b-c). In addition, sandstones show evidence of intergranular pressure dissolution along grains surface and quartz overgrowths (Fig. 9d). The dissolution leads to the generation of stylolite planes along

which stable minerals as sulphides (pyrite) and organic matter are concentrated (Fig. 9c). Grain contacts are predominantly concave-convex, with subordinate long and sutured contacts (Figs. 9e-f). The percentage of sutured grain contacts increases towards the base of the sections, where the action of chemical compaction predominates (Figs. 9e-f). Tangential contacts are only present in sandstones with abundant carbonate cement.

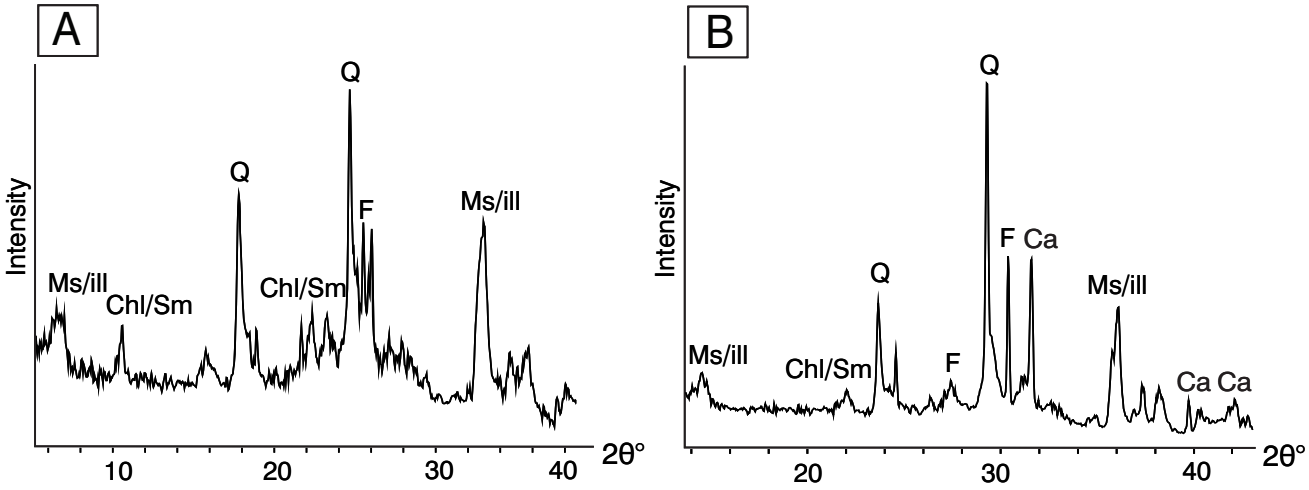

Figure 8. XRD diagrams of **a)** mudrcoks and **b)** tuffs, showing peaks of quartz (Q), feldspars (F), muscovite/illite (Ms/ill), chlorite/smectite (Chl/Sm) and calcite (Ca).

Cementation and replacement. Authigenic minerals are present as cements, filling the available space between grains and/or as partial or complete replacement of unstable grains. The main authigenic minerals in the studied samples are calcite and silicates, including zeolites, quartz, and feldspar overgrowths and clays (chlorite, illite/illite-smectite, muscovite, biotite). Furthermore, other accessory minerals precipitated during diagenesis as pyrite, prenithe, and epidote.

Cement constitutes from 5 to 25% of the total rock volume. Carbonate and zeolite cements are the most significant while quartz and feldspar overgrowths and clays cements are subordinated (Fig. 4a). The composition of cements varies throughout the sedimentary sections. The lower and middle sections are dominated by carbonates whereas in upper levels zeolitic cements predominate (Fig. 6a).

Calcite is one of the principal cements in the analysed sandstones. This cement constitutes between 3 to 25 % (average: 11 %) of the total composition of sandstones in the lower and middle levels, decreasing towards the top of the columns (<1 %) (Fig. 4a). Calcite mainly occurs as poikilotopic cement, forming a mosaic of coarse crystals surrounding the detrital grains (Fig. 10a) and subordinately as isolated pore-filling intergranular cement, with small (between 10-100 μm) crystals arranged between clasts (Fig. 10b). Coarse-grained calcites have dimensions of 100-500 μm (Fig. 10a). Calcite is also common as a replacement mineral, occurring as partial or complete replacement of feldspars and lithic fragments and rarely quartz grains (Fig. 10c).

Cathodoluminescence studies show different carbonate events reflected by changes in luminesce colours (Figs. 10d-f). Two phases of calcite cements can be distinguished: i) poikilotopic mosaic (Ca I) represented by coarse crystals with dull reddish luminescence (Figs. 10d-e) and, in less abundance, ii) pore-filling intergranular small crystals (Ca II) with bright orange luminescence (Fig. 10f). Replacement calcite also display different patterns. At least two replacement events were described: i) calcite as partial replacement of grains (lithics fragments and feldspars), with opaque orange luminescence (Ca R I; Figs. 10d-f), and ii) calcite as complete or partial replacement of grains (mainly lithics fragments), with bright reddish luminescence (Ca R II; Fig. 10e).

Zeolite cement is frequent at the upper part of the sections, constituting between 4 to 25% of the total sandstone composition (average: 10 %) (Fig.

4a). This cement is laumontite, which occurs as coarse crystalline poikilotopic mosaic, surrounding the detrital grains (Figs. 11a-b) and as isolated pore-filling intergranular cement, with small crystals arranged between grains (Fig. 11b). Laumontite also occur as partial or total replacement of feldspars or volcanic lithic fragments (Figs. 11b-c).

Cathodoluminescence studies show different carbonate events reflected by changes in luminesce colours (Figs. 10d-f). Two phases of calcite cements can be distinguished: i) poikilotopic mosaic (Ca I) represented by coarse crystals with dull reddish luminescence (Figs. 10d-e) and, in less abundance, ii) pore-filling intergranular small crystals (Ca II) with bright orange luminescence (Fig. 10f). Replacement calcite also display different patterns. At least two replacement events were described: i) calcite as partial replacement of grains (lithics fragments and feldspars), with opaque orange luminescence (Ca R I; Figs. 10d-f), and ii) calcite as complete or partial replacement of grains (mainly lithics fragments), with bright reddish luminescence (Ca R II; Fig. 10e).

Zeolite cement is frequent at the upper part of the sections, constituting between 4 to 25% of the total sandstone composition (average: 10 %) (Fig. 4a). This cement is laumontite, which occurs as coarse crystalline poikilotopic mosaic, surrounding the detrital grains (Figs. 11a-b) and as isolated pore-filling intergranular cement, with small crystals arranged between grains (Fig. 11b). Laumontite also occur as partial or total replacement of feldspars or volcanic lithic fragments (Figs. 11b-c).

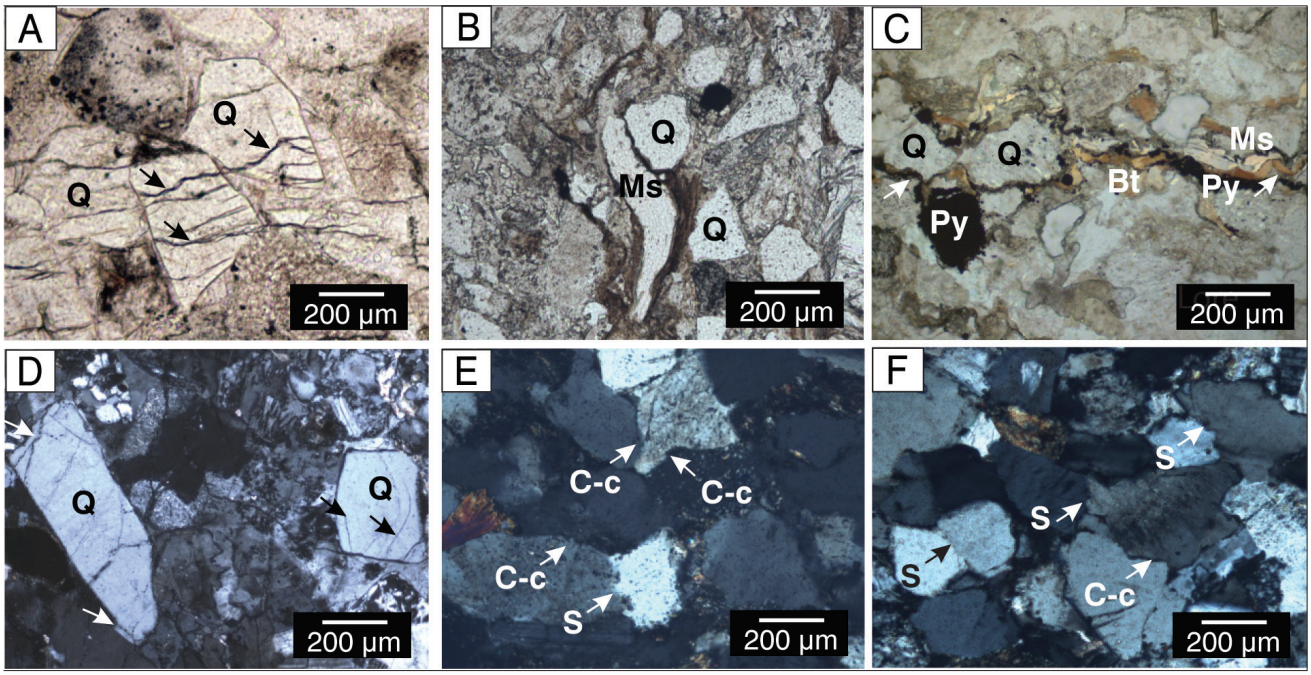

Figure 9. Thin-section photomicrographs of compaction features in Tunas Formation sandstones. **a)** Quartz (Q) grains fractured; **b)** Bent micas (muscovite, Ms and biotite, Bt) around resistant detrital quartz grains (Q); **c)** Dissolution planes (stylolites; showed by arrows) as a result of pressure dissolution with pyrite (py) and bent micas (Ms, Bt); **d)** intergranular pressure dissolution and quartz overgrowths (showed by arrows); **e-f)** Concave-convex (C-c) and sutured (S) grain contacts.

Quartz cement is common in analysed samples, present in low proportions (<1% of the total sandstone composition). This cement occurs as quartz overgrowths, around detrital quartz grains, showing optical continuity (Figs. 11d-e). In some cases, the overgrowths are highly developed with a width up to 40 μm (Fig. 11d), although in most cases the cement occurs as small isolated euhedral overgrowths (Figs. 11e-f).

Feldspar cement is subordinate. It occurs as authigenic growth around detrital feldspar grains (potassic feldspars or plagioclase; Figs. 11e-f), in optical continuity. Aided by the feldspar staining method (Bailey and Stevens, 1960) it was determined that the secondary growth is mostly albite.

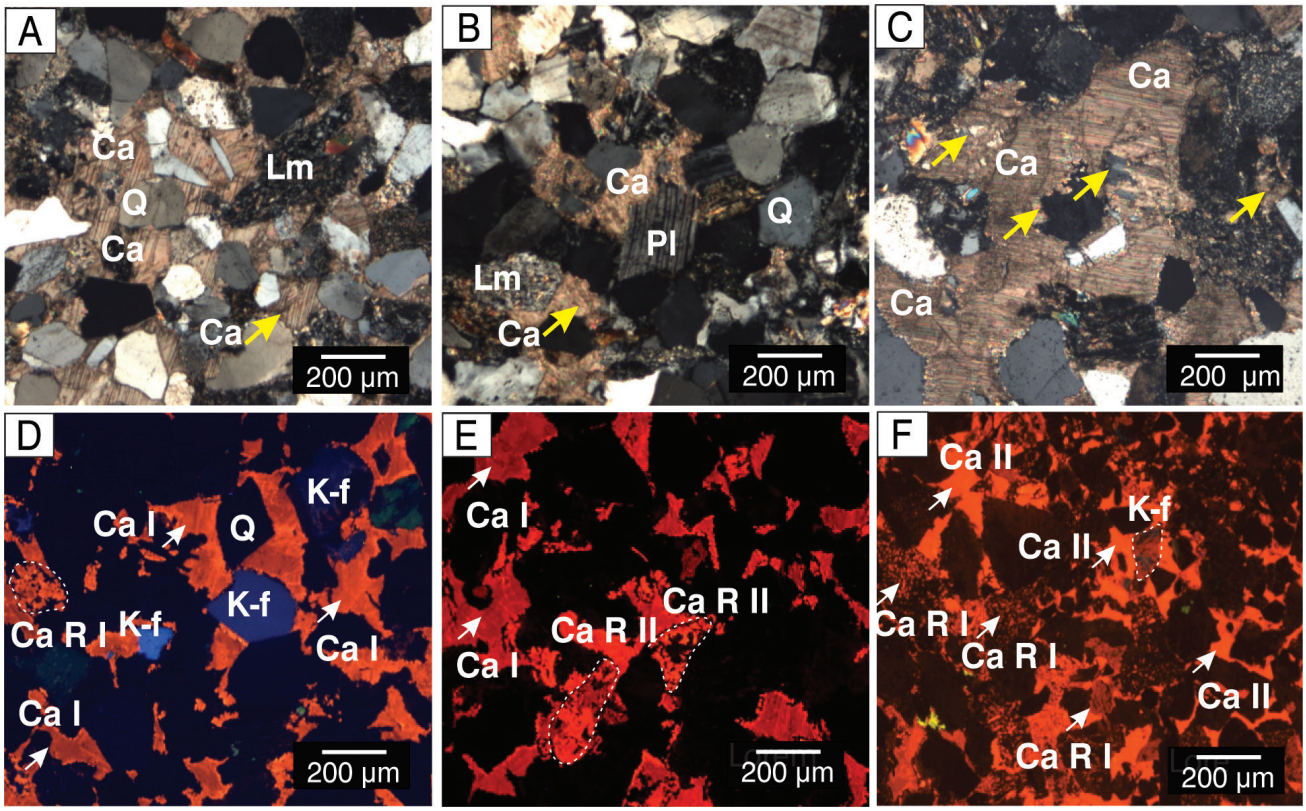

Figure 10. Thin-section photomicrographs of carbonate cement and replacement in Tunas Formation sandstones under transmitted light (a-c) and cathodoluminescence (d-f). Calcite (Ca) cement with **a)** poikilotopic mosaic texture, surrounding quartz grains (Q) and metamorphic lithic fragment (Lm) and **b)** blocky mosaic, with small crystals filling the space between quartz (Q), metamorphic lithic fragment (Lm) and plagioclase (Pl). **c)** Calcite (Ca) replacing unstable grains as total or partial replacement; **d-e)** Calcite cement with poikilotopic mosaic texture (Ca I), with dull reddish luminescence, surrounding quartz grains (Q) and potassic feldspars (K-f, blue luminescence), calcite as total or partial replacement of unstable grains with opaque orange luminescence (Ca RI) and bright reddish luminescence (Ca R II); **f)** Calcite cement with blocky mosaic texture (Ca II), with opaque orange luminescence and calcite (Ca R I) as replacement of lithic fragments and potassic feldspars (K-f).

Clay minerals are mostly observed as replacements of lithic fragments and feldspars and subordinately as matrix or cement (Figs. 11g-i). Illite and muscovite dominate the clay fraction at the basal levels while illite and chlorite become more abundant toward the middle and upper levels (Fig. 4a). Illite and sericite fill the poral space engulfing detrital grains (Figs. 11g-h). Sericite also alters feldspars (Fig. 11h). Biotite and muscovite occur as detrital and/or authigenic minerals, the latter recognized by their larger size (Figs. 11g-i). Occasionally, micas are bent and replaced by chlorite (Figs. 11g-i). Chlorite occurs as a detrital and/or authigenic mineral, often associated with epidote (Fig. 11i).

QEMSCAN analyses also helped to distinguish authigenic minerals (Fig. 12). Calcite and laumontite are easily distinguishable when they occur as cement or as grain replacements (Fig. 12). Conversely, quartz and feldspar overgrowth remain undetected since they occur as syntaxial overgrowths around detrital grains of the same composition. Moreover, QEMSCAN is a useful tool to identify the composition of clay minerals (Fig. 12), nevertheless, it is not easy to differentiate between their occurrence as pore-fills or grain-replacements.

Porosity. Porosity is secondary, generated by fracturing and dissolution of feldspars and carbonate cement (Fig. 13). No evidence of primary intergranular porosity was observed. Secondary porosity by fracturing is the most frequent, present in 60 % of the studied samples. Fractures can occur locally, as microfractures in detrital grains and/or cements, or throughout the entire sample, generating open spaces from 0.02 to 0.04 mm thick (Figs. 12c-d, 13a-c). Fractures are interconnected, surrounding the grains or crossing them, preferably in quartz grains and less frequently in feldspars and lithic

fragments (Figs. 12c-d, 13b-c). Fracture arrangement is generally parallel (horizontal) and to a lesser extent perpendicular or sub-perpendicular (vertical) to the stratification plane (Figs. 13a-c).

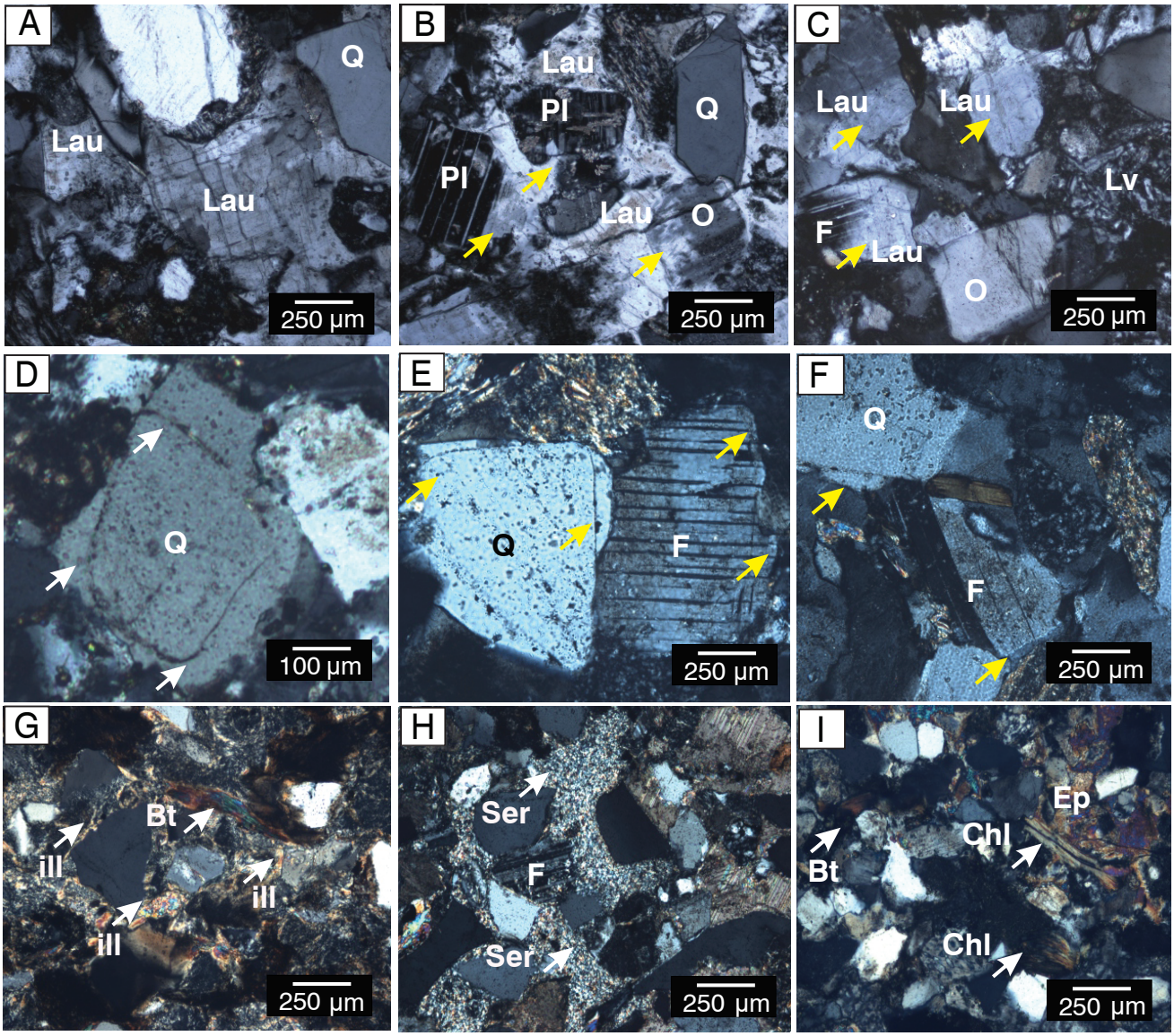

Figure 11. Thin-section photomicrographs of zeolites and clays as cement and replacement and quartz and feldspar overgrowths in Tunas Formation sandstones under transmitted light. **a)** Laumontite (Lau) cement with poikilotopic mosaic texture surrounding quartz grains (Q). **b-c)** Laumontite (Lau) cement with equicrystalline mosaic, with small crystals filling the space between feldspars (Plagioclase, Pl and Orthose, O) and laumontite as partial or complete replacement of feldspars (showed by arrows); **d-f)** Quartz (Q) and feldspars (F) grains with authigenic overgrowths (showed by arrows); **g-h)** Clay cement composed of illite (ill) and sericite (Se) and diagenetic biotite (Bt). Sericite occurs also replacing feldspars (F); **i)** Micas as detrital grains (biotite, Bt), authigenic chlorite (Chl) and epidote (Ep).

Secondary porosity by dissolution is found in 40 % of the studied samples, mostly observed towards the base of the sedimentary succession. Dissolution usually affects the unstable detrital grains as feldspars (Figs. 13d-e) or the carbonate cement (Fig. 13f). Dissolution of feldspars shows different degrees. Partial feldspar dissolution produces intragranular porosity (Fig. 13d) whereas complete feldspar dissolution produces intergranular porosity (Fig. 13e), with pores up to 100 μm. Similarly, dissolution of carbonate cement could be partial or total, the latter generating intergranular porosity

and interconnected pores (Fig. 13f). Some samples display intracrystalline porosity by dissolution of calcite cement or feldspars grains along twin planes. Thus, very small (2 μm) pores were generated within the crystals, with a minimal effect on the total porosity of the rock.

Visually determined porosity values vary from 0.1 to 4 % of the total rock volume, prevailing values less than 1 % (Table 2). In some samples, the visual porosity may be slightly overestimated as microfractures may have been created during thin section preparation, yielding values higher than those determined by petrophysical core analyses (i.e., sample M136; Table 2). QEMSCAN analyses yielded porosity values ranging from 0.09 to 2.03 % of the analyzed thin section (Table 2). From petrophysical core analyses, the porosity varies from 0.4 to 3.4 % and permeability ranges between 10-3 and 10-6 millidarcies (Table 2). The highest porosity corresponds to the highest permeability (Table 2).

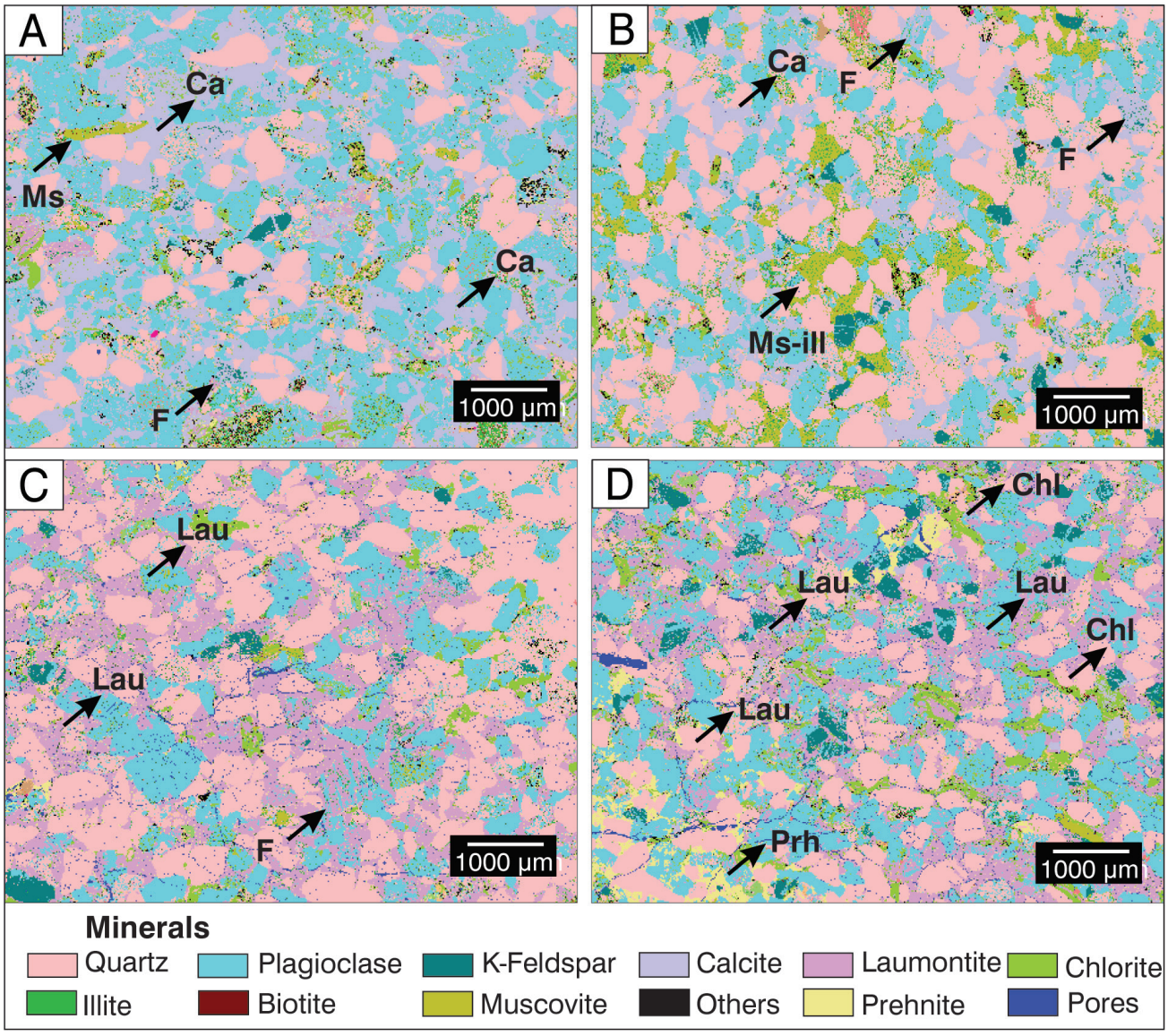

Figure 12. QEMSCAN analyses of authigenic minerals. **a-b)** Calcite (Ca) as poikilotopic cement and replacement of feldspars (F), muscovite (Ms) and muscovite-illite (Ms-ill); **c-d)** Laumontite (Lau) as poikilotopic cement and replacement of feldspars (F) and lithic grains, prehnite (Prh), and chlorite (Chl). Also, porosity (blue) generated by fractures could be distinguished.

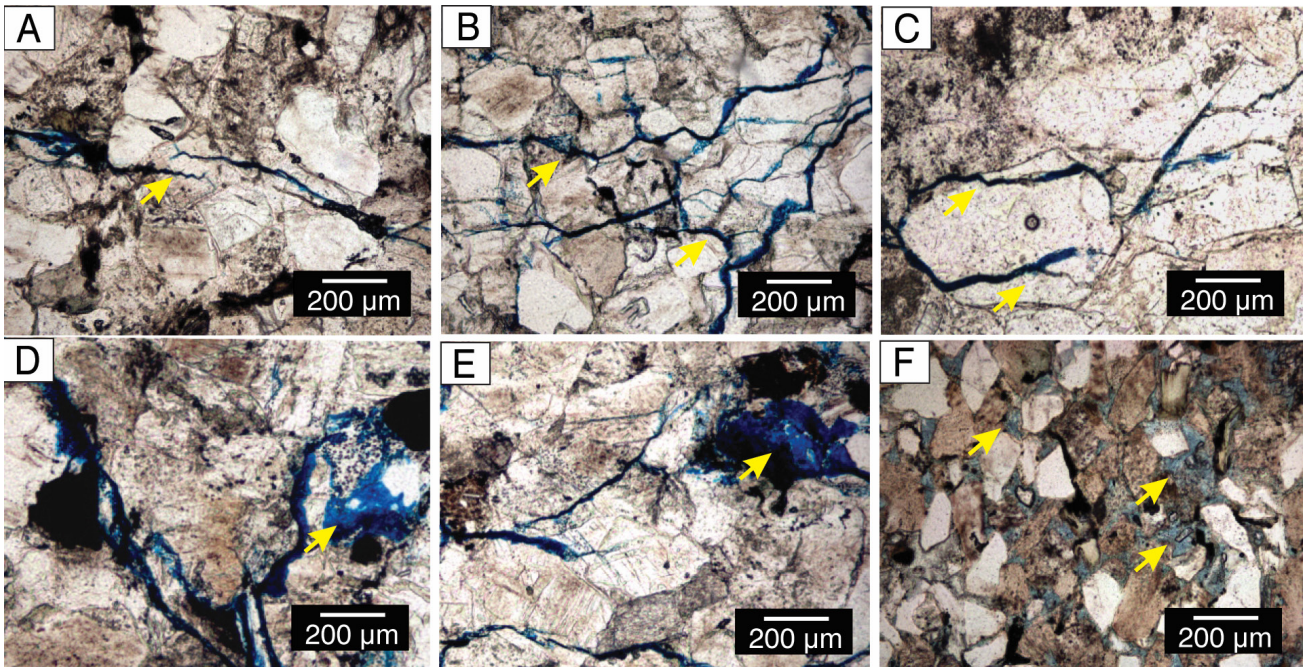

Figure 13. Thin-section photomicrographs of secondary porosity in Tunas Formation sandstones under transmitted light (showed by arrows). **a-c)** Secondary porosity by fracturing of detrital grains and cements. Fractures are interconnected, surrounding or crossing the grains; **d-f)** Secondary porosity by dissolution of feldspar grains intragranular (d) or intergranular (e); **f)** Secondary porosity by dissolution of carbonate cement.

Well	Sample	Depth	Optical porosity (%)	QEMSCAN porosity (%)	Porosity determined by CCA (%)	Permeability determined by CCA (%)	Porosity type
PANG 0001	509	304.55	0.2	-	-	-	Dissolution and fracture
	495	323.2	0.6	-	-	-	Dissolution and fracture
	458	365.6	-	1.5	-	-	Fracture and dissolution
	103a	822.8	0.25	-	-	-	Dissolution and fracture
	103b	821.5	-	1.64	-	-	Dissolution
PANG 0003	M377	182.4	0.45	2.03	-	-	Fracture and dissolution
	M368	198.9	-	1.41	-	-	Fracture
	M351	239.6	1.48	2.64	-	-	Fracture and dissolution
	M343	251.5	-	1.35	-	-	Fracture
	M315	311.5	no visual porosity	0.34	-	-	Fracture
	M261	492.6	-	0.11	-	-	Dissolution
	M248	516.3	no visual porosity	0.19	-	-	Fracture and dissolution

M212	601.0	2.48	-	-	-	Fracture and dissolution
M186	648.9	-	0.30	-	-	Fracture and dissolution
M137	732.5	-	-	0.44	14 E-4	Dissolution
M136	732.0	4	-	3.24	12 E-3	Dissolution
M117	757.2	no visual porosity	0.11	0.39	48 E-6	Dissolution
M54	838.3	no visual porosity	0.22	-	-	Dissolution
M47	846.3	0.5	-	1.87	14 E-4	Fracture and dissolution
M46	848.8	-	0.92	-	-	Dissolution and fracture
M38	854.8	no visual porosity	0.14	-	-	Dissolution
M35	860.6	-	0.88	-	-	Dissolution
M22	879.9	no visual porosity	0.13	-	-	Dissolution

Table 2. Results of porosity and permeability obtained by optical (microscopy), QEMSCAN and conventional petrophysical core analysis (CCA) and porosity type.

Fluid inclusions analysis

Petrography and fluorescence analysis. Petrography and fluorescence studies of fluid inclusions were performed in sandstones cements (carbonate and quartz overgrowths) and calcite and quartz veins in mudrocks (Fig. 3). Fluid inclusions of primary, pseudo-secondary, and secondary origin were recognized (Figs. 14, 15, 16). The composition of the fluid inclusions (aqueous or organic) was defined based on their fluorescence colour. Hydrocarbon-bearing inclusions show yellow to greenish fluorescence depending on the composition and maturity of the fluid trapped (Riecker, 1962; Burruss, 1981).

In calcite cements, primary fluid inclusions predominate, occurring as isolated or in groups (Figs. 14a-b). They have one (liquid) or two phases (liquid-vapor, with 90/10 and 80/20 ratios), rhombic and anhedral shapes and sizes from 2 to 8 μm (Fig. 14a, b). Occasionally, they show slight light blue fluorescence (Figs. 14b-c). Pseudo-secondary fluid inclusions are aligned in microfractures within the crystals. They present small size (<4 μm) and two phases (liquid-vapor) (Fig. 14d). In quartz overgrowths, pseudo-secondary inclusions predominate, aligned in growth planes of quartz grains (Fig. 14e, f).

Fluid inclusions of secondary origin were recognized in quartz grains in sandstones (Fig. 15) grouped in microfractures that crosscut more than one grain (Fig. 15). They present sizes from 2 to 12 μm, dark colors, and occasionally intense light blue and greenish fluorescence only in the liquid phase (Figs. 15c, f, h, j). Fluorescent fluid inclusions were only found in sandstones with dispersed organic matter, placed close to coal levels (samples M458, M47; Figs. 2-3).

In calcite veins, primary fluid inclusions occurred as isolated or in groups (Figs. 16a-d). They have one (liquid) or two phases (liquid-vapor with 90/10 and 80/20 ratios), rhombic and anhedral shapes and sizes from 4 to 15 μm (Figs. 16a-d). Occasionally, the inclusions show slight green to light blue fluorescence (Figs. 16b-d). Fluid inclusions of pseudo-secondary origin are aligned in microfractures within the crystals. They present sizes from 4 to 10 μm, two phases (liquid-vapor with 80/20 ratios) and occasionally intense light blue fluorescence (Figs. 16e-f). Fluid inclusions of secondary origin are aligned in microfractures that crosscut more than one quartz crystal (Figs. 16g-

h). They show small size (<4 μm), dark colors and intense green and light blue fluorescence (Figs. 16g-h).

In quartz veins, primary fluid inclusions predominate, occurring isolated or in groups (Figs. 16i-j). They have one (liquid) or two phases (liquid-vapor with 90/10, 80/20 and rarely 60/40 ratios), prismatic and anhedral shapes and sizes from 4 to 20 μm (Figs. 16i-k). Fluid inclusions of pseudo-secondary origin occur aligned in growth planes of quartz crystals. They show small sizes (2-6 μm) and one or two phases (liquid-vapor) (Fig. 16l). The inclusions in quartz veins did not show fluorescence (Fig. 16i-l).

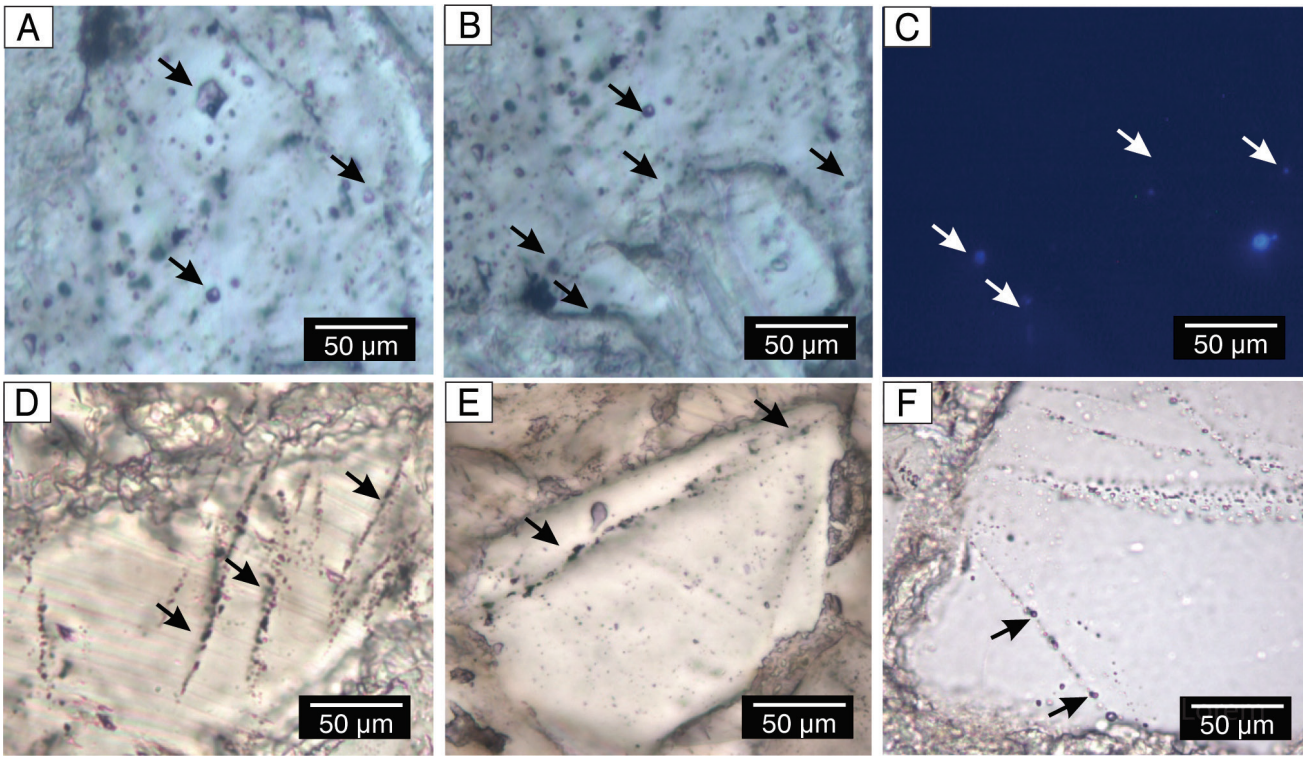

Figure 14. Thin-section photomicrographs of fluid inclusions in carbonate cement **(a-d)** and quartz overgrowths **(e-f)**. **a-c)** Primary fluid inclusions of one and two-phases, with weak light blue fluorescence **(c)**; **d)** Pseudo-secondary fluid inclusions clustered in microfractures; **e-f)** Pseudo-secondary fluid inclusions aligned along growth planes in quartz grains. Photomicrographs under transmitted light **(a-b, d-f)** and ultraviolet incident light (UV) **(c)**.

Fluid inclusion microthermometry. Homogenization temperatures (Th) were obtained in fluid inclusions hosted in sandstones cements (carbonate and quartz overgrowths) and calcite and quartz veins (Table 3). Workable fluid inclusions (> 6 μm) were difficult to find in calcite and quartz cements, thus, most of the data were obtained from calcite and quartz veins. In calcite cement, homogenization temperatures of primary fluid inclusions range from 128 to 168 °C, with predominant values < 150 °C (Table 3; Fig. 17a). In quartz cements, homogenization temperatures of pseudo-secondary fluid inclusions vary from 124 to 200 °C (Table 3; Fig. 17b). In calcite veins, homogenization temperatures of primary fluid inclusions vary widely from 119 to 200 °C, with two populations ranging from 120 to 140 °C and 150 to 180°C (Table 3; Fig. 17c). In quartz veins, homogenization temperatures of primary fluid inclusions range from 115 to 248 °C, with predominant values < 160 °C (Table 3; Fig. 17c).

DISCUSSIONS

Porosity generation over diagenetic history

Porosity in the Tunas Formation sandstones is mostly controlled by diagenetic and tectonic processes, which acted during their burial history

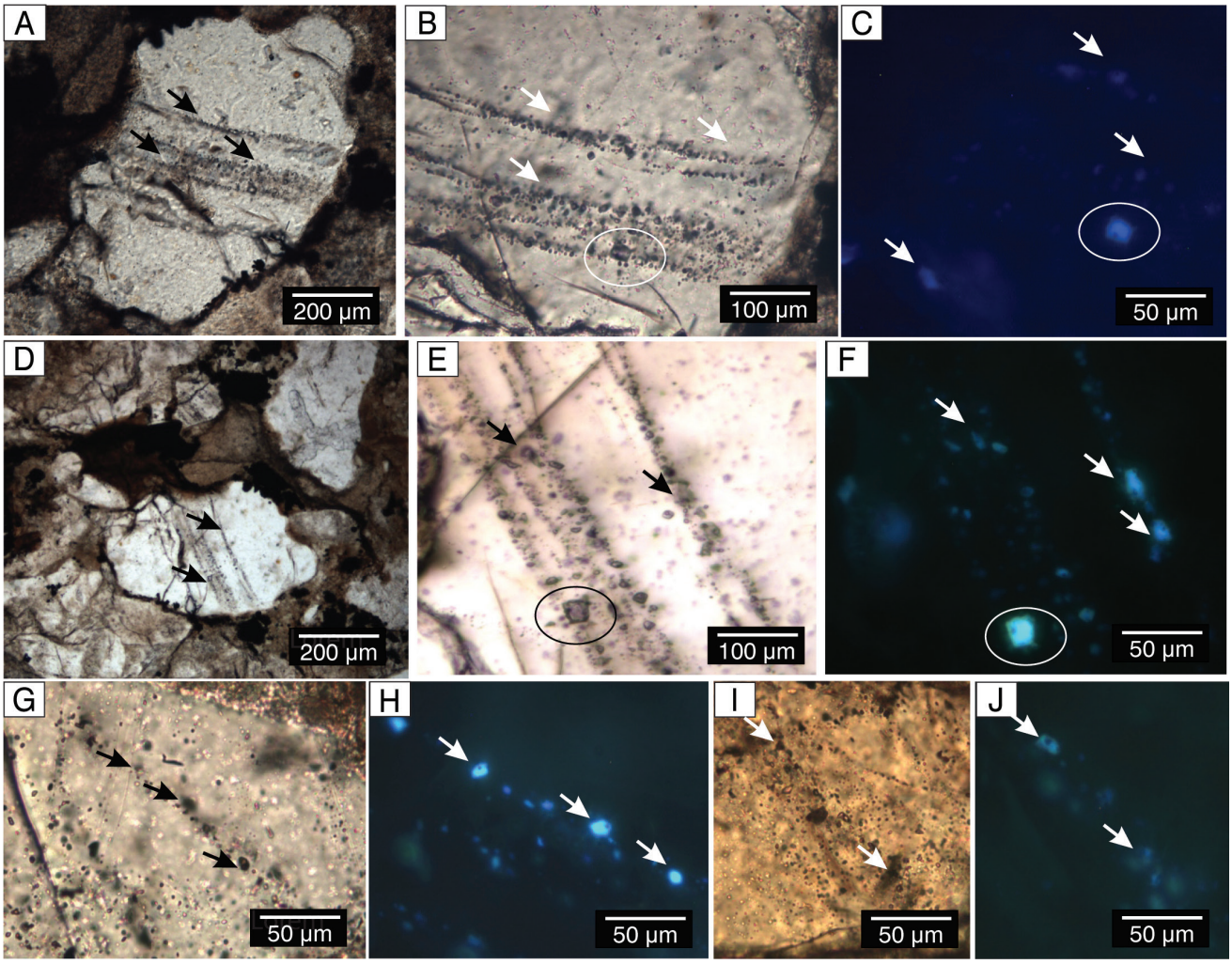

Figure 15. Thin-section photomicrographs of secondary origin fluid clustered in microfractures that crosscut more than one quartz grain. Fluid inclusions show intense light blue **(c, f, h)** and greenish fluorescence **(f, j)**. Photomicrographs under transmitted light **(a-b, d-e, g, i)** and UV **(c, f, h, j)**.

and subordinately by the composition of the clastic fraction.

Fracture secondary porosity is prevalent in the analyzed samples and is therefore considered the main process influencing overall porosity of the rock. The medium to fine-grained sandstone levels located towards the top (175 – 250 m) and the base (~ 700 m) of the analyzed sections display the highest porosity values by fracturing (Table 2; Figs. 2, 3). Fractures would have been generated by the tectonic stresses existing during the foreland stage of the basin and/or the lithostatic loading during burial of the sedimentary column (Arzadún *et al.*, 2016, 2021; Febbo *et al.*, 2021; Choque *et al.*, 2021, 2022). The stresses that affected the rock at different burial stages led to an increase in the brittle behavior of the sandstone grains (Gale *et al.*, 2014) and thus, in the fracturing of quartz and feldspars grains. Furthermore, the increase in pore pressure triggered during organic matter maturation and hydrocarbon generation would have favored the formation of natural fractures (Gale *et al.*, 2014; Fall *et al.*, 2015). The combination of these mechanisms resulted in the development of interconnected fracture networks that enhance the porosity and permeability of rocks and could act as pathways for hydrocarbon migration and accumulation. Indeed, the presence of hydrocarbon-bearing fluid inclusions hosted in microfractures in quartz grains and calcite veins (Figs. 14b-c, 15, 16a-h) demonstrate the relationship between hydrocarbons migration and accumulation and microfractures formation.

Dissolution is another important diagenetic process, which generates intra or intergranular

secondary porosity. This mechanism affected chemically unstable detrital grains as feldspars and lithic fragments and calcite cements. The dissolution degree depends on the chemical composition of the minerals and the chemical diagenetic environment. Carbonates and feldspars dissolution could be caused due to the action of carbonic acids derived from the maturation of the organic matter present in organic-rich levels (Blatt, 1979; Schmidt and McDonald, 1979). Consequently, this type of porosity is mainly present in sandstone layers strongly cemented with calcite, close to coal beds (Table 2; Fig. 4). Total dissolution of grains generates larger pore sizes (macropores) and a possible interconnection between them, increasing the porosity and permeability of the rock.

Sandstones with a high percentage of unstable components (feldspars and lithic fragments) generate higher secondary porosity by dissolution than those with stable minerals as quartz. The mineralogical composition of cements also influences porosity, with carbonate cement showing intra or intergranular secondary porosity by dissolution, whereas zeolite cements only present isolated intra-crystalline dissolution. Additionally, the precipitation of quartz and feldspar overgrowths is unfavorable for porosity development, since they are more stable to dissolution processes.

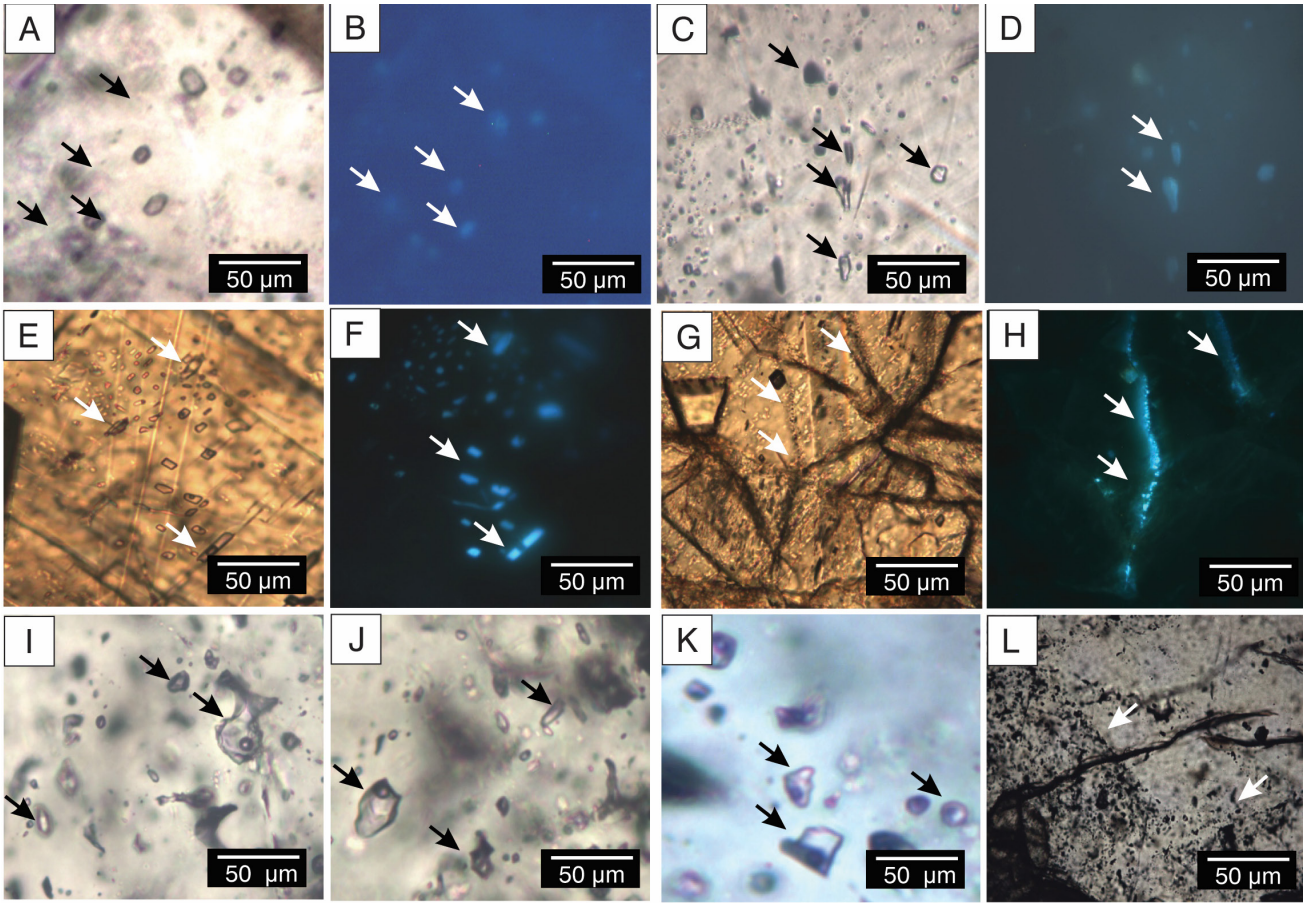

Figure 16. Thin-section photomicrographs of fluid inclusions in calcite **(a-h)** and quartz veins **(i-l). a-d)** Primary fluid inclusions of one and two-phases, with slightly light green and blue fluorescence **(b, d)** in calcite veins; **e-h)** Pseudo-secondary fluid inclusions aligned in microfractures within calcite crystals with intense light blue fluorescence **(f, h); i-k)** Primary fluid inclusions of one and two-phases in quartz veins; **l)** Pseudo-secondary fluid inclusions clustered in growth planes of quartz crystals. Photomicrographs under transmitted light **(a, c, e, g, i-l)** and UV **(b, d, f, h)**.

Sample	Diagenetic feature	Shape	Size (μm)	Homogenization temperature (°C)
M22	Calcite cement	Subhedral prismatic	4	128
		Subhedral prismatic	4	132
		Subhedral rhombic	6	132
		Subhedral rhombic	4	138
		Subhedral prismatic	4	138
		Subhedral rhombic	6	162
		Subhedral rhombic	8	168
		Subhedral prismatic	6	168
		Subhedral rhombic	6	>200
		Subhedral rhombic	4	>200
		Anhedral	4	>200
M261	Calcite cement	Subhedral prismatic	4	124
		Subhedral prismatic	4	138
		Subhedral rhombic	6	140
		Subhedral rhombic	6	162
M22	Quartz overgrowth	Subhedral rhombic	10	124
		Subhedral rhombic	10	127
		Subhedral prismatic	10	132
		Subhedral prismatic	10	150
		Subhedral prismatic	10	158
		Subhedral rhombic	8	198
		Subhedral rhombic	8	200
M41	Calcite vein	Subhedral prismatic	8	119
		Subhedral prismatic	6	125
		Subhedral rhombic	6	132
		Subhedral rhombic	6	145
		Anhedral	8	152
		Subhedral rhombic	15	166
		Subhedral rhombic	4	169
		Subhedral rhombic	4	169
		Subhedral rhombic	6	170
		Subhedral rhombic	6	182
		Subhedral rhombic	10	185
		Subhedral rhombic	10	186
		Anhedral	4	186
		Subhedral prismatic	10	187
		Subhedral prismatic	10	188
		Subhedral rhombic	6	189
		Anhedral	6	190
		Subhedral rhombic	6	200
		Subhedral prismatic	6	200

M92	Calcite vein	Subhedral rhombic	6	126
		Subhedral rhombic	6	126
		Subhedral prismatic	6	137
		Anhedral	8	154
		Subhedral rhombic	6	165
		Subhedral rhombic	10	186
		Anhedral	4	186
		Subhedral prismatic	10	187

Table 3. Homogenization temperatures in calcite and quartz cements and veins.

Reservoir quality

Reservoir quality mainly depends on the effective porosity (percentage of interconnected pores available to contribute to fluid flow) and the permeability of the rock. Other minor factors influencing in the reservoir quality are total organic carbon content (TOC%), thermal maturity of organic matter, lithological and mineralogical composition of the reservoir, fluid saturation, and formation pressure (Passey *et al.*, 2012). Additionally, the areal distribution of the reservoir, its thickness, and the proximity to the source rock are critical factors to consider. In the analyzed samples, mechanical and chemical compaction and early cementation resulted in a significant reduction in porosity, which negatively affected the reservoir quality of the Tunas Formation sandstones. Conversely, other processes as fracturing and intergranular dissolution are effective for the reservoir enhancement, since they generate interconnected pores allowing the migration and accumulation of fluids. Secondary porosity by intragranular or intracrystalline dissolution have a minor effect on the reservoir quality because they generate small pores mostly limited to a grain and therefore not interconnected.

In the studied samples, porosity is exclusively of the secondary type. Porosity values determined by optical, QEMSCAN, and petrophysical analyses range from 0.1 to 4 %, with those <1% predominating, and permeability is very low, from 10^{-3} to 10^{-6} millidarcies. Based on the obtained petrophysical parameters, sandstones of the Tunas Formation are classified as tight sandstones (Holditch, 2006; Meckel and Thomasson, 2008). Based on its high TOC % content (from 0.5 to 53.9 %; Febbo *et al.*, 2022a) coal-bearing levels of the Tunas Formation could be characterized as high-quality source rocks (Magoon, 1988). Additionally, vitrinite reflectance measurements (%Ro) ranging between 1.50 and 2.80 %, indicates a late oil to gas window for coal deposits (Arzadún *et al.*, 2017; Febbo *et al.*, 2023b). In concordance with %Ro data, homogenization temperatures obtained in fluid inclusions, mostly ranging between 160 and 200 °C (Fig. 17), confirm a metagenesis stage for the Tunas Formation. Moreover, fluorescence studies in fluid inclusions evidence the presence of hydrocarbons trapped within the inclusions (Burrus, 1981; Figs. 14b-c, 15, 16a-h). In summary, geochemical data, vitrinite reflectance, and fluid inclusions studies establish the potential of the coal-bearing levels of the Tunas Formation as gas source rocks. Based on these evidences, sandstone levels of the Tunas Formation would present potential as unconventional tight gas sandstone reservoirs, as these reservoirs are characterized by porosities <10 % and permeabilities <0.1 millidarcies (Magoon, 1988; Holditch, 2006). From the lithologies analyzed, naturally fractured and calcite-cemented sandstones close to coal levels, located between 700 and 850 m (Figs. 2-3), show the greatest potential for hydrocarbon storage as they have the highest porosity (4−0.5 %; Table 2) and permeability (10^{-3}−10^{-4} millidarcies; Table 2) values. Furthermore, the proximity of these sandstones to source rocks (coal/organic-rich shales) may favor the development of secondary porosity by fracturing and dissolution during the generation and migration of organic fluids. The mudrocks and very low permeability sandstones overlying the potential reservoir levels could act as seal rocks, contributing to the existence of stratigraphic type traps. Further petrophysical studies are needed to better define

reservoir levels and asses the elements of a potential petroleum system in the Claromecó Basin.

Diagenetic history of the Tunas Formation

Although it is difficult to constrain the precise timing and duration of the diagenetic processes, an overall diagenetic evolution for the Tunas Formation is proposed on the basis of petrographic textural relationships, diagenetic minerals, and fluid inclusion data (Fig. 18). The diagenetic history of this unit includes numerous and complex processes developed during the early diagenesis (eogenesis) and the mesogenesis.

During early diagenesis (up to 80 °C; Choquette and Pray, 1970), mechanical compaction occurred because of lithostatic loading pressure during burial, substantially reducing the pore space (Fig. 18). As a result, brittle grains would be fractured and micas bent. Increasing alkalinity during organic matter alteration (Berner, 1981) favoured the precipitation of poikilotopic calcite cement, developing relatively large crystals that occupied the space between framework grains. Early calcite cement precipitation was mostly related to the presence of decomposable organic matter and to a lesser extent to the dissolution of plagioclase and lithic fragments (Morad, 1998). Hence, calcite cement is better represented towards the bottom of the sequences where carbonaceous levels are located (Figs. 2-4). Moreover, during eogenesis, quartz and feldspar overgrowths can further reduce the depositional intergranular

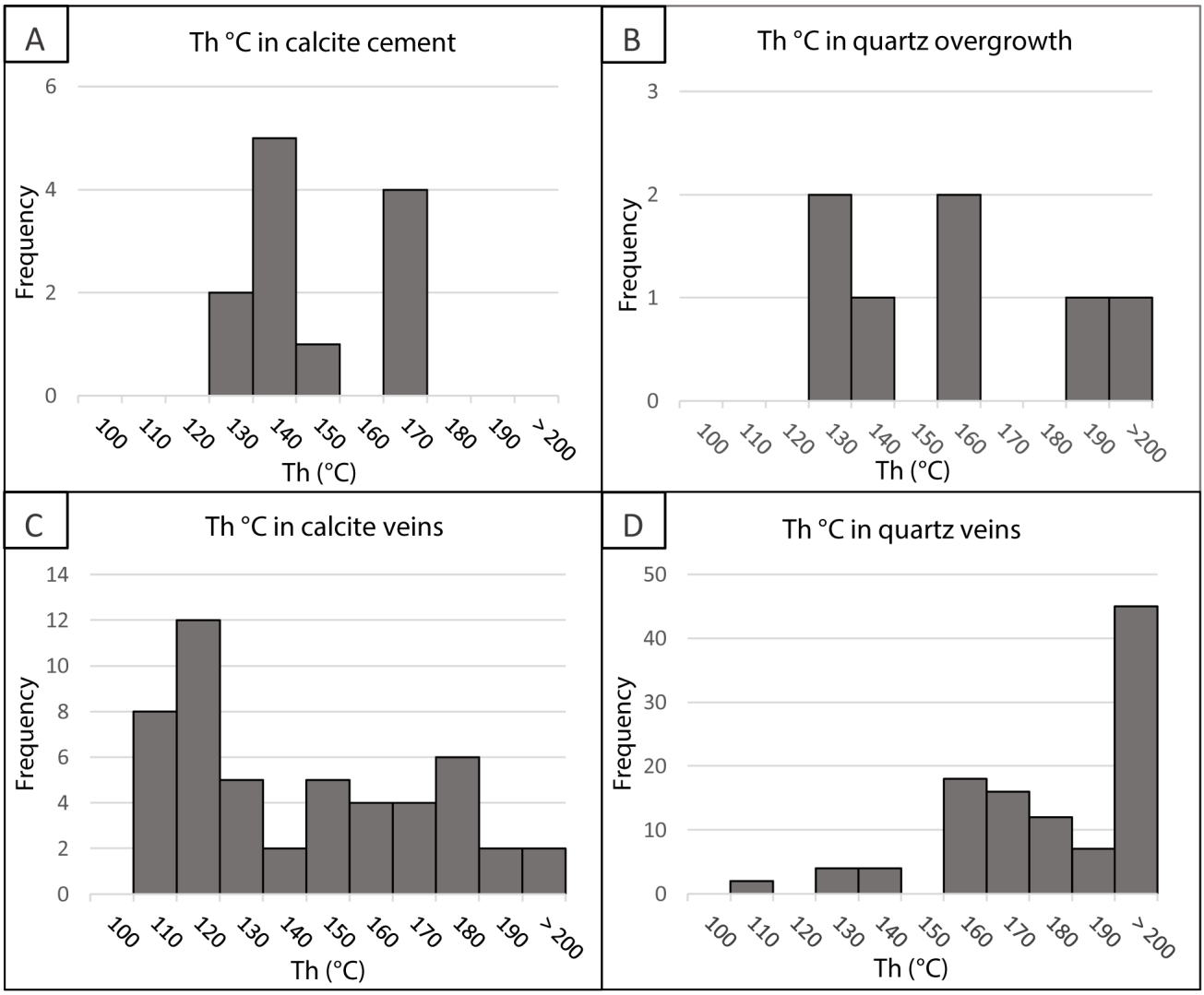

Figure 17. Homogenization temperature (Th °C) histogram of fluid inclusions trapped in **a)** Calcite cement (samples M22 and M261); **b)** Quartz overgrowth (sample M22); **c)** Calcite veins (samples M41 and M92); **d)** Quartz veins (sample M41)

space. Therefore, during early diagenesis most of the primary porosity is lost due the reduction of space between detrital grains caused by physical compaction and precipitation of early authigenic minerals (Fig. 18).

During mesogenesis (80 to 200 °C; Choquette and Pray, 1970) the most significant diagenetic changes occurred in the reservoir in response to increasingly high temperature and pressure. Important processes were chemical compaction and precipitation of authigenic minerals as cement, which further reduced the pore space (Fig. 18). Chemical compaction promoted concave-convex to sutured grain contacts, stylolite formation, and pressure dissolution. The latter mainly affects detrital quartz grains, increasing the concentration of silica in solution, which could migrate and precipitate later as secondary growths (Blatt, 1979). Based on

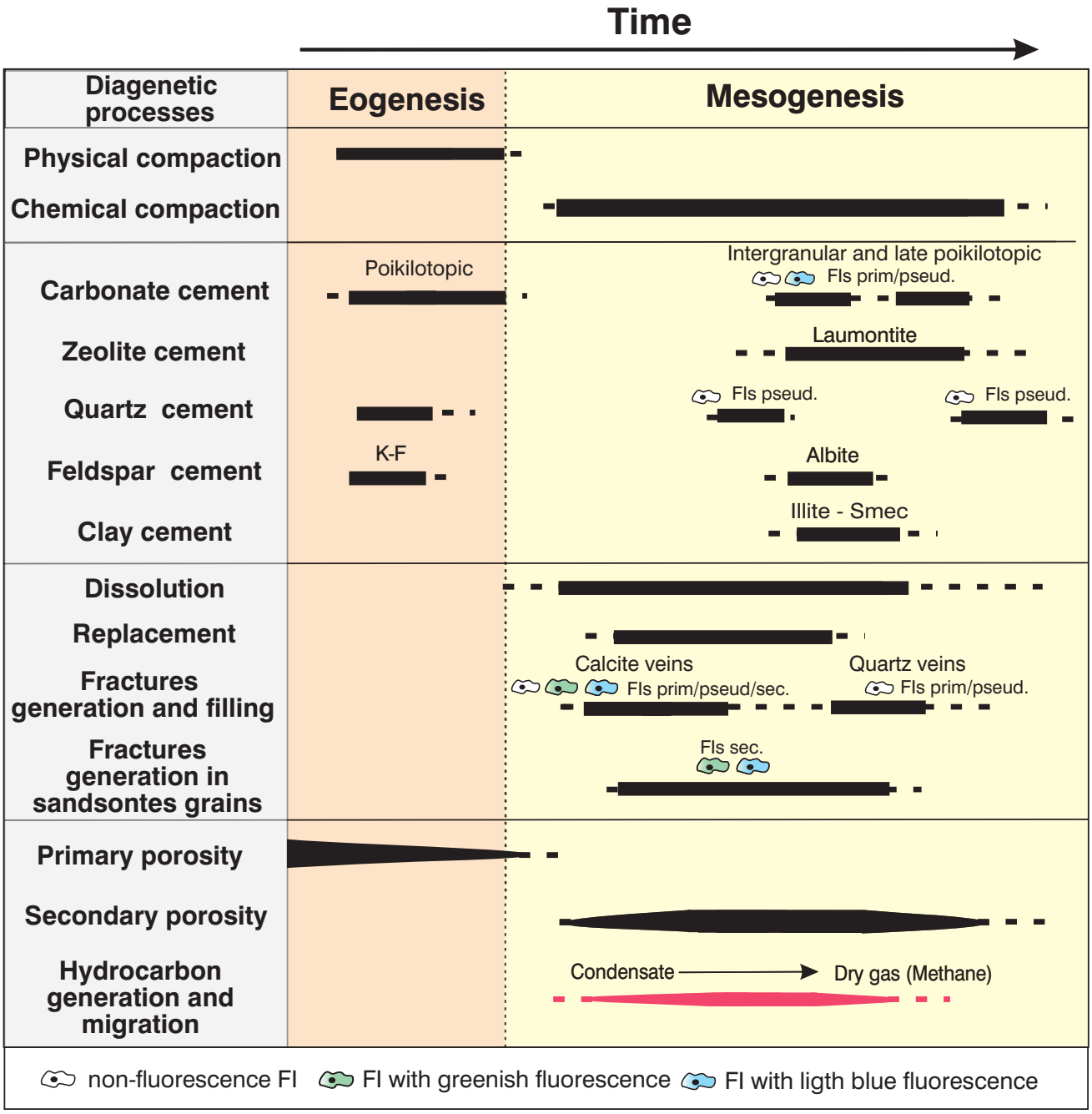

Figure 18. Paragenesis of the Tunas Formation. Fluid inclusions (FI) distributed in diagenetic features (cements, fractures, and veins) and fluorescence colours indicating hydrocarbon trapped in the inclusion are show (prim: primary, pseud: pseudosecundary, and sec: secondary origin).

homogenizations temperatures of fluid inclusions obtained in quartz overgrowths, quartz cements could be generated at different temperatures, leading to at least two precipitation events (Figs. 17, 18).

Changes in temperature, pressure, and pore fluid chemistry during mesogenesis resulted in the precipitation of authigenic minerals as cements or as replacement of unstable minerals (Fig. 18). Under this new conditions, calcite and zeolite cements with pore-filling intergranular textures and, to a lesser extent, quartz and albite overgrowths occurred (Fig. 18; Blatt, 1979; Surdam *et al.*, 1989). Zeolite cement is formed from the alteration of tuffs, plagioclases, and volcanic lithic fragments, therefore these cements are widespread towards the central and upper part of the section, where volcanic components are more abundant (Fig. 4; Hay, 1966). If the dissolution of pre-existing minerals was intense, late cements could develop poikilotopic textures. Fluid inclusion and cathodoluminescence data point out that calcite cements could precipitated at different temperatures, evidencing different stages of cementation (Figs. 17, 18). Alteration and corrosion mainly affected feldspars and lithic fragments, which were subsequently replaced by calcite, zeolites, or clay minerals (Fig. 18).

During the late mesogenesis stage, temperatures between 120 and 200 °C would have favored the maturation of organic matter of the carbonaceous levels leading to the generation of gaseous hydrocarbons (dry gas or methane; Tissot and Welte, 1984%; Arzadún *et al.*, 2017; Febbo *et al.*, 2002a; Febbo, 2023). At these temperatures, the release of acidic fluids during thermal decarboxylation (Schmidt and McDonald, 1979) favored the dissolution of carbonate cement and unstable detrital grains, which generated secondary porosity (Fig. 18). Additionally, other processes as tectonic stresses and pore-fluid pressure increase due to hydrocarbon generation and migration could contributed to secondary porosity generation by fracturing (Fig. 18). In some cases, fractures were filled by calcite or quartz. According to homogenizations temperatures measured in fluid inclusions, carbonate veins were formed between 120 and 190 °C (Figs. 17, 18) while quartz veinlets were generated at higher temperatures (Th > 160 °C; Figs. 17, 18). Fracture networks could have acted as hydrocarbon migration and accumulation pathways, as evidenced by the presence of hydrocarbon-bearing inclusions (Fig. 18).

CONCLUSIONS

The mineralogy and petrophysical properties of the Tunas Formation sandstones have undergone significant changes during diagenesis, affecting the reservoir quality. Analyzed sandstones show porosity values that ranges between 0.1 and 4 % and permeability from 10^{-3} to 10^{-6} millidarcies. Homogenization temperatures obtained from microthermometry studies range from 120 to 230 °C, confirming a late catagenesis to metagenesis stage for this unit, within the wet to dry gas window. Moreover, organic fluid inclusions with green and light blue fluorescence indicate the presence of organic components (hydrocarbons) within the inclusions. Taking into account the petrophysical characteristics of the rocks, sandstone levels placed near coal-bearing levels (source rocks), located at the base of the sedimentary columns, have potential as unconventional tight gas sandstone reservoirs.

During early diagenesis, mechanical compaction and precipitation of early calcite cements were the main processes that triggered to primary porosity reduction. Later on, during the mesogenesis stage, chemical compaction and precipitation of calcite and zeolite cements further contribute to porosity loss. However, secondary porosity was generated by fracturing and dissolution during this diagenetic stage. Fracture secondary porosity is prevalent in the analyzed samples, which could generate interconnected networks, contributing to increase the porosity and permeability of the rock. Fractures were developed as a consequence of burial and tectonic stresses and by the increase in pore pressure during the hydrocarbon generation and migration. Hydrocarbon-bearing fliud inclusions hosted in microfractures in quartz grains and calcite veins demonstrate the relationship between hydrocarbons migration and accumulation and microfracture formation. Additionally, dissolution of unstable grains and calcite cements caused by the action of acid fluids generated during the decomposition of organic matter favoured the generation of intra or intergranular porosity, improving reservoir quality. The reservoir properties in the Claromecó Basin have been controlled mainly by diagenetic processes and tectonic stress that acted during the burial of

the basin. These properties were also influenced by the composition of clasts and cements and presence of coal and carbonaceous shales, able to generate hydrocarbons.

Acknowledgments. The authors thank the Department of Earth Sciences of the University of Geneva, Switzerland, and Departamento de Geología, Universidad Nacional del Sur, Argentina, for providing the equipment and personnel to carry out sample analysis. The cores were donated to Universidad Nacional del Sur (UNS, Bahía Blanca, Argentina) by Rio Tinto Mining Exploring Company. Special thanks to the three reviewers, Dra. Maisa Tunik, Dr. Carlos Oscar Limarino and Dr. Oscar López-Gamundi, for their valuable suggestions and careful corrections of the manuscript, which have improved it considerably. This work was funded by Comisión de Investigaciones Científicas (CIC - PIT-AP-BA 2016/17/18) and Secretaría de Ciencia y Tecnología, Universidad Nacional del Sur, (SECYT-UNS - PGI24/H128) projects. The authors acknowledge support from the Federal Commission for Scholarships for Foreign Students for the award of the "Swiss Government Excellence Scholarship" and the Consejo Nacional de Investigaciones Científicas y Técnicas (CONICET) and Comisión de Investigaciones Científicas (CIC) for the Doctoral Scholarships.

REFERENCES

Alessandretti, L., Philipp, R.P., Chemale, F., Brückmann, M.P., Zvirtes, G., Metté, V. and Ramos, V.A. (2013). Provenance, volcanic record, and tectonic setting of the Paleozoic Ventania Fold Belt and the Claromecó Foreland Basin: Implications on sedimentation and volcanism along the southwestern Gondwana margin. *Journal of South American Earth Sciences*, 47: 12-31. http://dx.doi.org/10.1016/j.jsames.2013.05.006.

Andreis, R.R., Lluch, J.J. and Iñiguez Rodríguez, A.M. (1979). Paleocorrientes y paleoambientes de las Formaciones Bonete y Tunas, Sierras Australes de la Provincia de Buenos Aires, Argentina. *VI Congreso Geológico Argentino* Actas, 2: 207-224, Buenos Aires.

Andreis, R.R. and Japas, M.S. (1991). Cuenca de Sauce Grande y Colorado. *12° International Congress on Carboniferous and Permian Stratigraphy and Geology and Academia Nacional de Ciencias* Actas, 45-64, Córdoba.

Aoyagi, K. and Kazama, T. (1980). Transformational changes of clay minerals, zeolites and silica minerals during diagenesis. *Sedimentology*, 27, (2): 179-188.

Archangelsky, S. and Cúneo, R. (1984). Zonación del Pérmico continental de Argentina sobre la base de sus plantas fósiles. *III Congreso latinoamericano Paleontológico* Actas, 143-153, Ciudad de México.

Archangelsky, S., Azcuy C.L., Césari, S.N.; González, C.R., Hünicken, M.A., Mazzoni, A. and Sabattini, N. (1996). Correlación y edad de las biozonas. In: S. Archangelsky (Eds.). *El Sistema Pérmico en la República Argentina y en la República Oriental del Uruguay, Academia Nacional de Ciencias*, 203-226.

Arzadún, G., Tomezzoli, R.N. and Cesaretti N.N. (2016). Tectonic insight based on anisotropy of magnetic susceptibility and compaction studies in the Sierras Australes thrust and fold belt (southwest Gondwana boundary, Argentina). *Tectonics*, 35: 1015-1031. https://doi.org/10.1002/2015TC003976.

Arzadún, G., Cisternas, M.E., Cesaretti, N.N. and Tomezzoli, R.N. (2017). Presence of charcoal as evidence of paleofires in the Claromecó Basin, Permian of Gondwana, Argentina: Diagenetic and paleoenvironment analysis based on coal petrography studies. *GeoResJ*, 14: 121-134. https://doi.org/10.1016/j.grj.2017.11.001.

Arzadún, G., Lovecchio, J.P., Becchio, R., Uriz, N.J., Cingolani, C., Febbo, M.B., Hernandez, R., Bolatti, N. and Kress, P. (2020). Thermochronology of the Ventana Ranges and Claromecó Basin, Argentina: Record of Gondwana breakup and South Atlantic passive margin dynamics. *Journal of South American Earth Sciences*, 105, 102965. https://doi.org/10.1016/j.jsames.2020.102965.

Arzadún, G., Tomezzoli, R.N., Fortunatti, N., Cesaretti, N.N., Febbo, M.B. and Calvagno, J.M. (2021). Deformation understanding in the Upper Paleozoic of Ventana ranges at southwest Gondwana boundary. *Scientific Reports*, 11, 20804. https://doi.org/10.1038/s41598-021-99087-1.

Arzadún, G., Tomezzoli, R.N., Trindade, R., Gallo, L.C., Cesaretti, N.N. and Calvagno, J.M. (2018). Shrimp zircon geochronology constrains on Permian pyroclastic levels, Claromecó Basin, south-west margin of Gondwana, Argentina. *Journal of South American Earth Sciences*, 85: 191-208.

Azcuy, C.L. and Caminos, R. (1987). Diastrofismo. In: Archangelsky, S. (Ed.), *El Sistema Carbonífero en la República Argentina, Academia Nacional de Ciencias*, 239-251.

Bailey, E. H., and Stevens, R. E. (1960). Selective staining of K-feldspar and plagioclase on rock slabs and thin sections. *The American Mineralogist*, 45: 1020-1025.

Ballivián Justiniano, C.A., Comerio, M.A., Gerónimo, O., Sato, A.M., Coturel, E.P., Naipauer, M. and Basei, M.A.S. (2020). Geochemical, palaeontological, and sedimentological approaches of a syn-orogenic clastic wedge: Implications for the provenance of the Permian (Cisuralian) Tunas Formation, Ventania System (Argentina). *Journal of South American Earth Sciences*, 104, 102836. https://doi.org/10.1016/j.jsames.2020.102836.

Beard, D.C. and Weyl P.K. (1973). Influence of Texture on Porosity and Permeability of Unconsolidated Sand. *American Association Petroleum Geologists Bulletin*, 57 (2): 349-369. https://doi.org/10.1306/819A4272-16C5-11D7-8645000102C1865D

Berner, R. (1981). A New Geochemical Classification of Sedimentary Environments. *Journal Sedimentary Petrology*, 51: 359-365.

Bjørlykke, K. and Høeg, K. (1997). Effects of burial diagenesis on stresses, compaction and fluid flow in sedimentary basins. *Marine and Petroleum Geology*, 14 (3): 267-276. https://doi.org/10.1016/S0264-8172(96)00051-7.

Blatt, H. (1979). Diagenetic processes in sandstones. In: P.A. Scholle and Schluger (Eds.) Aspect of diagenesis. *Society of Economic Paleontologists & Mineralogists*, Special Publication, 26: 141-158.

Buggisch, W. (1987). Stratigraphy and very low grade metamorphism of the Sierras Australes of the province of Buenos Aires, Argentina and implications in Gondwana correlations. *ZentralBlattt Mineralogie Geologie Paläontologie*, 1: 819-837.

Burruss, R.C. (1981). Hydrocarbon fluid inclusions in studies of sedimentary diagenesis. *Short Course in Fluid Inclusions: Applications to Petrology*, (Eds.) Hollister L. S. y M. L. Crawford, Min. Ass. Canada Short Course Handbook, 6:138-156.

Cade, C., Evans, I. and Bryant, S. (1994). Analysis of permeability controls: A new approach. *Clay Minerals*, 29 (4): 491-501. doi:10.1180/claymin.1994.029.4.08

Catuneanu, O., Hancox, P.J. and Rubidge, B.S. (1998). Reciprocal flexural behaviour and contrasting stratigraphies: a new basin development model for the Karoo retroarc foreland system, South Africa. *Basin Research*, 10: 417-439

Choque, G., Fortunatti, N.B, Febbo, M.B., Caruso, S., Tomezzoli, R.N. and Cesaretti, N.N. (2021). Fracturación estratigráfica en la Formación Tunas (pozo PANG 0003), Cuenca de Claromecó, Buenos aires, Argentina. *Revista de la Asociación Geológica Argentina*, 79 (2): 258-274.

Choque, G., Fortunatti, N. B, Febbo, M. B. and Tomezzoli, R.N. (2022). Fracture frequency and anisotropy of magnetic susceptibility: A case of study in the Claromecó Basin (PANG 0003 well), southwestern Gondwana boundary. *Journal of South American Earth Sciences*, 120. https://doi.org/10.1016/j.jsames.2022.104094

Choquette, P.W. and Pray, L. (1970). Geologic nomenclature and classification of porosity in sedimentary carbonates. *American Association Petroleum Geologists Bulletin*, 54: 207-250.

Cobbold, P.R. and Massabie, A., Rossello, E.A. (1986). Hercynian wrenching and thrusting in the Sierras Australes foldbelt, Argentina. *Hercynica*, II, 2: 135–148.

Compton, R.R. (1962). *Manual of Field Geology*, Wiley, London, UK.

Cúneo, N.R. (1996). Permian phytogeography in Gondwana. *Palaeogeography, Palaeoclimatology, Palaeoecology*, 125: 75--104.

di Pasquo, M., Di Nardo, J., Martínez, M., Arzadún, G. and Silvestri, L. (2018). Análisis palinoestratigráfico de muestras de subsuelo de la Formación Tunas (Pérmico), Cuenca de Claromecó, Provincia de Buenos Aires, Argentina. *XVII Simposio Argentino de Palinología y Paleobotánica, Boletín de la Asociación Latinoamericana de Paleobotánica y Palinología* Actas, 77-78, Paraná.

Du Toit, A.L. (1927). A geological comparison of South America with South Africa. *Carnegie Institution of Washington Publication*, 381: 1-157.

Du Toit, A.L. (1937). Our Wandering Continents. Oliver and Boyd, London, 366 pp.

Fall, A., Eichhubl, P., Bodnar, R.J, Laubach, S.E. and Davis, J.S (2015). Natural hydraulic fracturing of tight-gas sandstone reservoirs, Piceance Basin, Colorado. *GSA Bulletin*, 127 (1-2): 61-75. https://doi.org/10.1130/B31021.1

Febbo, (2023). *Análisis diagenético y de anisotropía de susceptibilidad magnética en registros de subsuelo pérmicos de la Formación Tunas: pozos PANG 0001 y PANG 0003, Cuenca de Claromecó, Buenos Aires, Argentina*. Tesis doctoral, Universidad Nacional del Sur, Argentina, 353 pp. (inédito).

Febbo, M.B., Omodeo-Salé, S. and Moscariello, A. (2023). Thermal evolution of the Permian Claromecó foreland Basin (southern Gondwana, Argentina) based on organic petrology and basin modelling. *36th IAS International Meeting of Sedimentology* Actas, 285, Dubrovnik, Croatia.

Febbo, M.B., Arzadún, G., Cesaretti, N.N., Tomezzoli, R.N. and Fortunatti, N. (2022a). The Claromecó Frontier Basin: Hydrocarbon source rock potential of the Tunas Formation, southwestern Gondwana margin, Argentina. *Marine and Petroleum Geology*, 137, 105491. https://doi.org/10.1016/j.marpetgeo.2021.105491.

Febbo, M. B., Tomezzoli, R.N., Cesaretti, N.N., Choque, G., Fortunatti, N. and Arzadún G. (2022b). Paleotectonic setting during Permian sedimentation in the Claromecó Foreland Basin, southwestern Gondwana margin (Buenos Aires, Argentina). *Journal of Paleogeography*, 11 (3): 427-447. https://doi.org/10.1016/j.jop.2022.06.001.

Febbo, M.B., Tomezzoli, R.N., Calvagno, J.M., Arzadún, G., Gallo, L. and Cesaretti, N.N. (2021). Anisotropy of magnetic susceptibility analysis in Tunas Formation cores (Permian), Claromecó Basin, Buenos Aires, Argentina: Its relation to depositional and post-depositional conditions. *Journal of South American Earth Sciences*, 107, 103144. https://doi.org/10.1016/j.jsames.2020.103144.

Febbo, M.B., Fortunatti, N., Cesaretti, N.N., Arzadún, G. and Tomezzoli, R.N. (2018). Evolución diagenética de la Formación Tunas para el pozo PANG 0001, Cuenca de Claromecó, provincia de Buenos Aires, Argentina: Su potencial como reservorio de hidrocarburos. *X Congreso de Exploración y Desarrollo de Hidrocarburos* Actas, 763-779, Mendoza.

Folk, R.L., Andrews, P.B. and Lewis, D.W. (1970). Detrital sedimentary rock classification and nomenclature for use in New Zeland. *New Zeland Journal of Geology and Geophysics*, 13: 937-968.

Furque, G. (1973). Descripción geológica de la Hoja 34n, Sierra de Pillahuincó, Provincia de Buenos Aires. *Boletín del Servicio Nacional de Minería y Geología* 141, 70, Buenos Aires.

Gale, J., Laubach, S., Olson, J., Eichhuble, P. and Fall, A. (2014). Natural Fractures in shale: a review and new observations. *American Association of Petroleum Geologist Bulletin*, 98 (11): 165-2216.https://doi.org/10.1306/08121413151.

Geel, C., De Wit, M., Booth, P., Schulz, H.M. and Horsfield, B. (2015). Palaeo-environment, diagenesis and characteristics of Permian black shales in the Lower Karoo Supergroup flanking the Cape Fold Belt near Janesville, Eastern Cape, South Africa: implications for the shale gas potential of the Karoo Basin. *South African Journal of Geology*, 118 (3): 249-274. doi:10.2113/gssajg.118.3.249.

Goldstein, R.H. and Reynolds, T.J. (1994). Systematics of fluid inclusions in diagenetic minerals. *Tulsa, Oklahoma, EUA, SEPM Short Course*, 31, 199 pp.

Gottlieb, P., Wilkie, G., Sutherland, D., Ho-Tun, E., Suthers, S., Perera, K., Jenkins, B., Spencer, S., Butcher, A. and Rayner, J. (2000). Using quantitative electron microscopy for process mineralogy applications. *JOM*, 52: 24-25. https://doi.org/10.1007/s11837-000-0126-9.

Grasetti, C.G., Piqué, T., Noya, M., Vila, G.S., Manoni, R., Brisson, I., De Leo D., Dzelalija, D, Canale, N., Zalazar, M, Cabana, C., Tunik, M., Fortunatti, N., Lebinson, F., Bahía, M. and Grill, S. (2022). Atlas AR-CO 2. An Argentinian atlas for underground CO 2 storage potential. *16th International Conference on Greenhouse Gas Control Technologies* Actas, Lyon, France.

Harrington, H.J. (1947). Explicación de las Hojas Geológicas 33m y 34m, Sierras de Curamalal y de la Ventana, Provincia de Buenos Aires. *Servicio Nacional de Minería y Geología, Buenos Aires*, 61, 43 pp.

Harrington, H.J. (1970). Las Sierras Australes de Buenos Aires, República Argentina: Cadena aulocogénica. *Revista de la Asociación Geológica Argentina*, 25 (2): 151-181.

Hay, R.L. (1966). Zeolites and zeolitic reactions in sedimentary rocks. *Geological Society of America Special paper*, 85: 1-130.

Holditch, S.A. (2006). Tight gas sands. *Journal of petroleum Technology*, 58 (06): 86-93.

Holz, M., França, A.B., Souza, P.A., Iannuzzi, R. and Rohn, R.A. (2010). Stratigraphic chart of the Late Carboniferous/Permian succession of the eastern border of the Paraná Basin, Brazil, South America. *Journal of South American Earth Sciences*, 29: 382-399.

Introcaso, A. (1982). Características de la corteza en el positivo bonaerense: Tandilia-Cuenca Interserrana-Ventania a través de datos de gravedad. *Observatorio Astronómico Municipalidad de Rosario, Publicación del Instituto de Física de Rosario*, 8: 1-6, Rosario.

Kalkreuth, W., Levandowski, J., Weniger, P., Krooss, B., Prissang, R. and Lima da Rosa, A. (2020). Coal characterization and coalbed methane (CBM) potential of the chico - lomã coalfield, Paraná Basin, Brazil - results from exploration borehole CBM001- CL - RS. *Energy Exploration & Exploitation*, 1-42. https://doi.org/10.1177%2F0144598720931167.

Keidel, J. (1916). La geología de las Sierras de la provincia de Buenos Aires y sus relaciones con las montañas del Cabo y los Andes. *Ministerio de agricultura de la Nación. Sección Geología, Mineralogía y Minería* Anales, 9 (3): 5-57, Buenos Aires.

Keidel, J. (1921). Sobre la distribución de los depósitos glaciares del Pérmico conocidos en la Argentina y su significación para la estratigrafía de la serie del Gondwana y la paleogeografía del Hemisferio Austral. *Academia Nacional de Ciencias*, 25: 239-368

Kostadinoff, J. (2007). Evidencia geofísica del umbral de Trenque Lauquen en la extensión norte de la cuenca de Claromecó, provincia de Buenos Aires. *Revista de la Asociación Geológica Argentina*, 62 (1): 69-75.

Kostadinoff, J. and Prozzi, C. (1998). Cuenca de Claromecó. *Revista de la Asociación Geológica Argentina*, 53 (4): 461-468

Langford R.P. (1992). Permian coal and paleogeography of Gondwana. *Paleogeography*, 39: 165.

Kollenz, S., Glasmacher, U.A., Rossello, E.A., Stockli, D.F., Schad, S. and Pereyra, R.E. (2017). Thermochronological constrains in the Cambrian to recent geological evolution of the Argentine passive continental margin. *Tectonophysics*, 716: 182-203.

Lesta, P. and Sylwan, C. (2005). Cuenca de Claromecó. *VI Congreso de Exploración y Desarrollo de Hidrocarburos, Simposio Frontera Exploratoria de la Argentina Actas*, 217-231, Mar del Plata.

López-Gamundi, O.R. (1996). Modas detríticas del Grupo Pillahuincó (Carbonífero tardío-Pérmico), Sierras Australes de la Provincia de Buenos Aires: su significado geotectónico. *Revista de la Asociación Argentina de Sedimentología*, 3 (1):1-10.

López-Gamundi, O.R. (2006). Permian plate margin volcanism and tuffs in adjacent basins of west Gondwana: Age constraints and common characteristics. *Journal of South American Earth Sciences*, 22: 227-238.

López-Gamundi, O.R. and Rossello, E.A. (2021). The Permian Tunas Formation (Claromecó Basin, Argentina): Potential naturally fractured reservoir and/or coal bed methane (CBM) play?. *Marine and Petroleum Geology*, 128: 1-14. https://doi.org/10.1016/j.marpetgeo.2021.104998.

López-Gamundi, O.R., Fildani, A., Weislogel, A. and Rossello, E. (2013). The age of the Tunas Formation in the Sauce Grande basin-Ventana foldbelt (Argentina): Implications for the Permian evolution of the southwestern margin of Gondwana. *Journal of South American Earth Sciences*, 45: 250-258.

López-Gamundi, O.R., Conaghan, P.J., Rossello, E.A. and Cobbold, P.R. (1995). The Tunas Formation (Permian) in the Sierras Australes Foldbelt, east central Argentina: Evidence for syntectonic sedimentation in a foreland basin. *Journal of South American Earth Sciences*, 8 (2): 129-142. https://doi.org/10.1016/0895-9811 (95)00001-V.

Lovecchio, J.P., Rohais, S., Joseph, P., Bolatti, N.D., Kress, P.R., Gerster, R. and Ramos, V.A. (2018). Multistage rifting evolution of the Colorado basin (offshore Argentina): Evidence for extensional settings prior to the South Atlantic opening. *Terra Nova*, 30: 359-368. https://doi.org/10.1111/ter.12351.

Magoon, L.B. (1988). Petroleum system of the United States. U.S. *Geological Survey, Bulletin 1870*. Denver, Co. 68 pp.

Meckel, L.D. and Thomasson, M.R. (2008). Pervasive tight-gas sandstone reservoirs: An overview. In: S.P. Cumella, K.W. Shanley, and W. K. Camp, (Eds.), *Understanding, exploring, and developing tight-gas sands*. Vail Hedberg Conference: AAPG Hedberg Series, 3, 13-27.

Mendonça Filho, J.G., Sommer, M.G., Klepzig, M.C., Mendonça, J.O., Silva, T.F. and Kern, M.L. (2013). Permian carbonaceous rocks from the Bonito Coalfield, Santa Catarina, Brazil: organic facies approach. *International Journal of Coal Geology*, 111: 23-36.

Milani, E.J. and De Wit, M.J. (2008). Correlations between the classic Paraná and Cape Karoo sequences of South America and southern Africa and their basin infills flanking the Gondwanides: Du Toit revisited. *Geological Society, London, Special Publications*, 294: 319-342.

Molina, A., Choque, G., Fortunatti, N. and Rainoldi, A. (2023). Potencial en el subsuelo de la provincia de Buenos Aires para la inyección de CO2: estudio preliminar en la Cuenca de Claromecó. *1° Conferencia Argentina de Captura, Utilización y Almacenamiento de CO2*, 41, La Plata.

Monteverde, A. (1937). Nuevo yacimiento de material pétreo en González Chaves. *Revista Minera*, 8, 116-124.

Morad, S. (1998). Carbonate cementation in sandstones: distribution patterns and geochemical evolution. In S. Morad (Ed.), *Carbonate Cementation in Sandstones*, 1-26. Wiley.

Morad, S., Al-Ramadan, K., Ketzer, M. and De Ros, L. (2010). The impact of diagenesis on the heterogeneity of sandstone reservoirs: A review of the role of depositional facies and sequence stratigraphy. *American Association Petroleum Geologists Bulletin*, 94 (8): 1267-1309.

Pángaro, F., Ramos V.A. and Pazos, P.J., 2015. The Hesperides basin: A continental-scale Upper Paleozoic to Triassic basin in southern Gondwana. *Basin Research*, 28: 685-711. https://doi.org/10.1111/bre.12126.

Pángaro, F. and Ramos, V.A. (2012). Paleozoic crustal blocks of onshore and offshore central Argentina: New pieces of the southwestern Gondwana collage and their role in the accretion of Patagonia and the evolution of Mesozoic South Atlantic sedimentary basins. *Marine and Petroleum Geology*, 37 (1): 162-183. http://dx.doi.org/10.1016/j.marpetgeo.2012.05.010.

Passey, Q.R., Bohacs, K.M., Esch, W.L., Klimentidis, R. and Sinha, S. (2012). My source rock is now my reservoir-Geologic and petrophysical characterization of shale-gas reservoirs. *American Association Petroleum Geologists Search and Discovery Article*, 90124.

Ramos, V.A. (1984). *Patagonia: Un nuevo continente paleozoico a la deriva?*. IX Congreso Geológico Argentino Actas, 311-325, Bariloche.

Ramos, V.A. (2008). Patagonia: A Paleozoic continental drift?. *Journal of South American Earth Sciences*, 26: 235-251. https://doi.org/10.1016/j.jsames.2008.06.002.

Ramos, V.A., and Kostadinoff, J. (2005). La cuenca de Claromecó. In: de Barrio, R.E., Echeverri, R.O., Caballé, M.F., Llambías, E., (Eds.). *Geología y recursos minerales de la provincia de Buenos Aires. XVI Congreso Geológico Argentino Relatorio*, 473-480, La Plata.

Ramos, V.A. and Naipauer, M. (2014). Patagonia: Where does it come from?. *Journal of Iberian Geology*, 40: 367-379. https://doi.org/10.5209/rev_JIGE.2014.v40.n2.45304.

Ramos, V.A., Chemale, F., Naipauer, M. and Pazos, P.J. (2014). A provenance study of the Paleozoic Ventania System (Argentina): Transient complex sources from western and eastern Gondwana. *Gondwana Research*, 26:719-740. https://doi.org/10.1016/j.gr.2013.07.008.

Shanmugam, G. (1984). Secondary porosity in sandstones: basic contributions of Chepikov and Savkevich. *American Association Petroleum Geologists Bulletin*, 68 (1): 106-107.

Shanmugam, G. (1990). Porosity prediction in sandstones using erosional unconformities. *American Association of Petroleum Geologist Memoir*, 49: 1-23.

Schmidt, V. and McDonald, D.A. (1979). The role of secondary porosity in the course of sandstone diagenesis. In: P.A. Scholle and Schluger (Eds.) *Aspect of diagenesis. Society of Economic Paleontologists & Mineralogists, Special Publication*, 26: 159-173.

Suero, T. (1972). Compilación geológica de las Sierras Australes de la provincia de Buenos Aires. *Anales LEMIT* Serie II, 3: 135-147, La Plata.

Surdam, R.C., Crossey, L.J., Hagen, E.S. and Heasler, H.P. (1989). Organic-inorganic interactions and sandstone diagenesis. *American Association of Petroleum Geologist Bulletin*, 73: 1-23.

Taylor, J.M. (1950). Pore-space reduction in sandstones. *American Association of Petroleum Geologist Bulletin*, 34 (4): 701-716.

Tissot, B. and Welte, D.H. (1984). *Petroleum Formation and Occurrence*. Second edition Springer- Verlag, Heidelberg. 669 pp.

Tohver, E., Weil, A.B., Solum, J.G. and Hall, C.M. (2008). Direct dating of chemical remagnetizations in sedimentary rocks, insights from clay mineralogy and 40Ar/39Ar age analysis. *Earth and Planetary Science Letters*, 274: 524-530.

Tomezzoli, R.N. (1999). La Formación Tunas en las Sierras Australes de la Provincia de Buenos Aires. Relaciones entre sedimentación y deformación a través de su estudio paleomagnético. *Revista de la Asociación Geológica Argentina*, 54 (3): 220-228.

Tomezzoli, R.N. (2001). Further palaeomagnetic results from the Sierras Australes fold and thrust belt, Argentina. *Geophysical Journal International*, 147: 356-366. https://doi.org/10.1046/j.0956-540x.2001.01536.x.

Tomezzoli, R.N. (2012). Chilenia y Patagonia: ¿un mismo continente a la deriva?. *Revista de la Asociación Geológica Argentina*, 69 (2): 222-239.

Tucker, M.E. (1981). *Sedimentary petrology: an introduction to the origin of sedimentary rocks.* Blackwell Scientific Publications, Oxford, 253 pp.

Vazquez Lucero, S.E., Prezzi, C., Scheck-Wenderoth, M., Bott, J., Gomez Dacal, M.L., Balestrini, F.I. and Vizán, H. (2020). 3D gravity modelling of Colorado and Claromecó basins: New evidences for the evolution of the southwestern margin of Gondwana. *International Journal of Earth Sciences*, 110: 2295-2313. https://doi.org/10.1007/s00531-020-01944-3.

Riecker, R.E. (1962). Hydrocarbon fluorescence and migration of petroleum. *American Association Petroleum Geologists Bulletin*, 46 (1): 60-75.

Roedder, E. (1984). Fluid inclusions. *Reviews in Mineralogy*, 12, Mineralogical Society of America, 644 p.

von Gosen, W., Buggisch, W. and Krumm, S. (1991). Metamorphism and deformation mechanisms in the Sierras Australes fold and thrust belt (Buenos Aires province, Argentina). *Tectonophysics*, 185: 335-356. https://doi.org/10.1016/0040-1951(91)90453-Y

Worden, R.H., and Burley, S.D. (2003). *Sandstone diagenesis: the evolution of sand to stone.* Sandstone diagenesis: Recent and ancient, 4, 3-44.

Zambrano, J.J. (1969). Cuencas sedimentarias en el subsuelo de la provincia de Buenos Aires y zonas adyacentes. R*evista de la Asociación Geológica Argentina*, 29: 443-469.

Zavala, C.A., Santiago, M.F. and Amaolo, G.E. (1993). Depósitos fluviales en la Formación Tunas (Pérmico). Cuenca Paleozoica de Ventania, provincia de Buenos Aires. *Revista de la Asociación Geológica Argentina*, 48: 307-316.

Zavala, C., Torresi, A., Zorzano A., Arcuri, M. and Di Meglio, M. (2019). Análisis sedimentológico y estratigráfico de la Formación Tunas (Pérmico, Cuenca de Claromecó). Estudio de subsuelo de los pozos PANG0001 y PANG0003. *Revista de la Asociación Geológica Argentina*, 76 (3), 296-314.